

Blast Loading of Sandwich Structures and Composite Tubes

H. Arora, P.A. Hooper, and J.P. Dear

Abstract This chapter reviews blast impact experimentation on glass fibre reinforced polymer (GFRP) and carbon-fibre reinforced polymer (CFRP) sandwich composite materials and laminate composite tubes. Explosive charges of 0.64–100 kg TNT equivalent were used during these air- and underwater-blast tests. The difference in response and damage inflicted from underwater- and air-blast loading was assessed from strain-field measurements and post-blast specimen analysis. Procedures for monitoring the structural response of such materials during blast events have been devised. High-speed photography was employed during the air-blast loading of GFRP and CFRP sandwich panels, in conjunction with digital image correlation (DIC), to monitor the deformation of these structures under shock loading. Failure mechanisms have been revealed using DIC and confirmed in post-test sectioning. The improved performance of composite sandwich structures with CFRP skins compared to GFRP equivalent constructions is demonstrated for air-blast experiments. Strain gauges were used to monitor the structural response of similar sandwich materials and GFRP tubular laminates during underwater shocks. The effect of the supporting/backing medium (air or water) of the target facing the shock has been identified during these studies. Mechanisms of failure have been established such as core crushing, skin/core cracking, delamination and fibre breakage. Strain gauge data supported the mechanisms for such damage. A transition in behaviour was observed in the sandwich panels when subject to an underwater blast as opposed to an air-blast load. Damage mechanisms notably shifted from distributed core shear failure originating from regions of high shear in air blast to global core crushing in underwater blast. The full-scale experimental results presented here will assist in the development of analytical and computational models. Furthermore, the research highlights the importance of boundary conditions with regards to blast resistant design.

H. Arora • P.A. Hooper • J.P. Dear (✉)

Department of Mechanical Engineering, Imperial College, London SW7 2AZ, UK

e-mail: hari.arora04@imperial.ac.uk; p.hooper07@imperial.ac.uk; j.dear@imperial.ac.uk

Keywords Air blast • Underwater blast • Shock • Sandwich structures • Composites

1 Introduction

The study reported here forms part of a programme to investigate the retention of integrity of composite structures subject to increasingly demanding conditions. When designing against such threats one has to consider the blast event (pressure wave), the surroundings (fluid medium and boundary conditions) and the component (material properties and construction). The research presented here focuses on air-blast loading of glass-fibre reinforced polymer (GFRP) and carbon-fibre reinforced polymer (CFRP) sandwich composite panels and underwater-blast loading of GFRP sandwich composite panels and GFRP tubular laminates.

It is clear from the nature of an explosion that they can be very damaging to a structure and it is because of recent events, accidental or otherwise, that there has been a growth within this area of research [1]. When a shock wave reaches a structure there are typically three stages of response that a structure undergoes. The first stage is where compressive stress waves are transmitted from the front face to the back. In polymer foam core sandwich fibre reinforced polymer composites, as those of primary concern for this investigation, core crushing occurs as well as impulsive transverse shear reaction forces initiating from the clamped edges. The structure does not experience any global deflection in stage 1. Momentum and kinetic energy are transmitted globally to the plate at the end of stage 1 while the transverse shear strains propagate towards the middle of the structure. By stage 2 the load pressure pulse would have decayed to negligible magnitudes. Meanwhile the transverse shear stress waves cause the development of bending and shear deformations behind the wave front. There comes a point in stage 3 where the direction of those shear waves reverse causing a reversal of plate deflection (at the point of maximum central point deflection) and flexural oscillations begin [2]. There have been numerous investigations into blast loading of structures using open-air charges, buried charges and other apparatus. Several studies have investigated dynamic deformations due to explosive blast loading on plates. Neuberger [3, 4] highlighted several early studies, which classified failure modes of structures under impulse loading, from large inelastic deformation to tearing and shear failure at the supports. Neuberger also highlighted various studies investigating the scaling effects for comparison of similar blast events using different explosive mass or specimen distance to quantify material response. These studies observed the effect of air-blast [3] and buried charges [4] on clamped circular plates and the validity of scaled testing. Several earlier studies have also investigated the dynamic deformations due to explosive blast loading on plates. Menkes and Opat [5] classified failure modes of structures under impulse loading, from large inelastic deformation to tearing and shear failure at the supports. Nurick amongst others has conducted extensive studies over the years investigating various plate response to blast loading summarised in

reference [6]. For instance the types of failures described by Menkes and Opat have been investigated further by Nurick, Olsson et al. [7], in particular the significant effects of the boundary conditions for the purpose of predicting tearing in steel plates have been highlighted in reference [8].

Cantwell, Nurick and Langdon et al. have continued similar experimental investigations and analysis into composite behaviour under blast conditions [9–11]. In addition to explosive testing, shock tubes have been found to give a good and convenient option for shock/blast studies. The advantage of shock tubes is the controlled nature of the event produced, in addition to the event concentrating solely on the shock wave influence rather than any others inherent with blast situations e.g. burning. A shock tube consists of a long rigid cylinder, divided into a high-pressure driver section and a low pressure driven section, which are separated by a diaphragm. A shock is created by pressurising one section (high-pressure) until the pressure difference across the diaphragm reaches a critical value, resulting in the diaphragm rupturing. This rapid release of gas creates a shock wave, which travels down the tube and on to the test specimen [12]. Tekalur et al. [12–14] have experimentally studied the effect of blast loading using shock tubes and controlled explosion tubes loading on E-glass fibre based composites and other materials. Results suggested that the E-glass fibre composite experienced progressive damage during high-rate loading of the same nature as described in Hoo Fatt and Palla [2], with progressive front-face failure due to indentation followed by complete core collapse. These studies have been continually developed by the same research group to great effect, with many parameters being examined such as the distribution of blast energy during the impact process [15] and retention of integrity of sandwich structures due to blast loads [16].

Changing the medium used to carry the shock from a gas to a liquid (increasing the density) increases speed of sound and generates a significant rise in pressures produced by a blast event. It is for these and related reasons that underwater shocks and their interaction with surrounding submerged structures are of particular interest to the naval industry. When an explosion occurs underwater, there is an intense release of energy, high pressure and heat, similar to the air blast case. This is relieved by the formation of an intense (compressive) pressure wave, or shock wave, which radiates away from the source. However with an underwater explosion, there is also the formation of high-pressure gas bubble, which is formed by the expanding reaction products formed during the explosion. The pressure within this bubble is significantly higher than hydrostatic and therefore the bubble radius increases rapidly. However, due to inertial and other effects, the gas bubble expands too far until the hydrostatic pressure is greater than the pressure within the gas bubble. The bubble then contracts once more until it contracts too far. The pressure in the gas bubble then rises in pressure and emits a compressive pressure wave prior to expanding once more from this minimum. There are a series of overshoots and undershoots during this process until all the energy is dissipated in one way or another. The movement and dynamic behaviour of the bubble is influenced by a number of factors including the proximity to the air-water interface, other surfaces and turbulence [17]. In terms of energy released, approximately 47% goes towards the formation

and pulsation of the bubble and the remainder to the shock wave [18]. If stand-off distance can be assumed to be large, then the effect of the bubble can be ignored, and this seems to be the focus of most authors, highlighted by Panciroli and Abrate [19].

Conducting underwater explosive experiments is again a very high risk and high cost procedure. Moreover, considerable care is needed to instrument underwater explosive experiments to obtain the required high quality data. Therefore, different laboratory experimental techniques are employed by researchers. For example, the principle of a shock tube has been applied to water blast simulations using the water-hammer effect. Deshpande et al. [20] investigated the fluid structure interaction (FSI) of sandwich plates with steel face sheets and aluminium foam cores. A strong FSI effect was observed experimentally and a coupled finite element (FE) analysis was able to capture the measured degree of core compression unlike the decoupled analysis, which underestimated the degree of core compression. This illustrated the importance of FSI and having a coupled analysis during such events. This water hammer technique has been used elsewhere incorporating moiré shadow interferometry techniques to obtain full field out-of-plane deformation profiles by Espinosa et al. [21]. This method was also employed by LeBlanc and Shukla [22] with in-depth finite element (FE) analyses forming agreements in terms of damage generated in the composite laminates studied. Other effects of water pertinent to naval structures are shock focusing during impacts, water slamming and wave interactions. This phenomenon has been investigated within a comprehensive study of impulse loading on marine structures conducted by Ravichandran et al. [23].

The complexity of blast load conditions is significant and various aspects are being investigated every day with the aim of improving computational simulations and hence the design process for marine structures. This investigation aims to highlight the mechanisms of failure observed within commercially available naval materials and improve the understanding behind the sequence of events responsible for such damage. The main focus of this study is the blast response of composites and sandwich structures on a large scale but related research [24–27] has focussed on the impact performance of composites and sandwich structures.

Although a significant amount of work is being conducted over a range of scales and types of experimentation, as highlighted in this chapter already, suitable standards for scaling and test procedures have not been established. Therefore data that is most valuable to industry is full-scale explosive testing and will be of focus for this investigation. Methods of instrumentation and sample restraint for large-scale marine structures will also be of focus, highlighting the precautions required to implement the traditional instrumentation methods and more modern techniques currently in use in a number of related research areas.

2 Materials

There were three different types of sandwich composite panels and one type of composite tubular laminate evaluated; these are shown schematically in Fig. 1. The sandwich panels had GFRP skins or CFRP skins on two different SAN cores

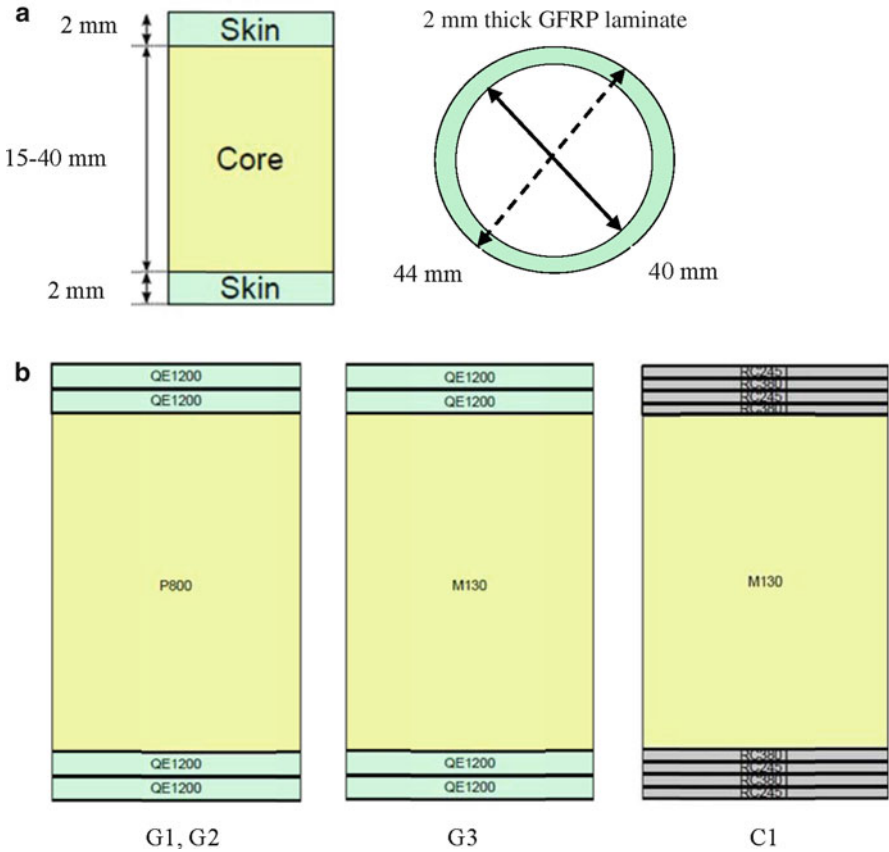


Fig. 1 Target constructions: (a) sandwich panels (*top left*) and tubular laminate (*top right*); (b) Sandwich panel skin lay ups for each type of panel tested: G1 & G2 (QE1200 glass skin with 40 mm P8 core and 30 mm P8 core respectively) – *left*; G3 (QE1200 glass skin with 25 mm M130 core) – *centre*; C1 (RC245T/RC380T carbon skins with 25 mm M130 core) – *right*

(P800 or M130). The GFRP-skinned sandwich panels were constructed using 2 plies of ($0^{\circ}/90^{\circ}/\pm 45^{\circ}$) E-glass quadriaxial skins with (manufacturer code QE1200) on SAN foam cores (manufacturer code P800 or M130) infused with an Ampreg 22 epoxy resin. Various core thicknesses were tested from 15 to 40 mm for air blast and underwater blast studies. The CRFP-skinned sandwich panels consisted of two repeat layers of two plies of $0^{\circ}/90^{\circ}$ carbon (code: RC245T) on two plies of $\pm 45^{\circ}$ carbon (code: RC380T) on a 25 mm thick SAN foam core (code: M130) and this was compared with GFRP-skinned sandwich panels consisting of 2 plies of ($0^{\circ}/90^{\circ}/\pm 45^{\circ}$) E-glass quadriaxial skins on a 25 mm thick SAN foam core (code: M130). All these sandwich constructions were infused with an Ampreg 22 epoxy resin. These different sandwich constructions are shown schematically in Fig. 1. A 3 mm thick panel made of mild steel (composition: EN-10025-2-05-S275JR-AR) was also tested for comparison with the 25 mm SAN foam-cored sandwich panels.

Comparisons can be made against the mild steel plate to compare conventional against more modern ship building materials and clarify what savings can be made, if any, on a weight-for-weight basis, for each sample construction. The GFRP and CFRP-skinned panels had equivalent mass per unit area, $\sim 17 \text{ kg/m}^2$. The steel plate also had a near equivalent mass per unit area as the composite sandwich panels, larger at $\sim 23 \text{ kg/m}^2$, and was included to demonstrate the advantages or otherwise of the composite sandwich construction over traditional engineering materials.

The exposed target areas for the air-blast and underwater-blast experiments were $1.6 \times 1.3 \text{ m}$ and $0.4 \times 0.3 \text{ m}$ respectively. The two different sized panels were designed to have a comparable aspect ratio. The larger panels, used for the air-blast, were to represent full-scale face-panels of comparable magnitude to real naval structures. Smaller samples were required for the underwater blast experiments to allow for sufficient rigid edge restraint/support during tests as well as manoeuvrability of the entire rig during test set-up. The smaller targets were used to keep the experiments within sensible bounds of the test facility in terms of the size of test pond, explosives used, desired maximum pressures and hence blast parameters (suitable guidelines for such underwater test designs are outlined in reference [28]). The process used to decide each of these factors started with the charge size, using a charge size and location in the test facility that minimised unwanted secondary pressure cycles from reflections etc. Secondly the size of the panel was chosen to allow sufficient damage to be inflicted by such a charge, whilst keeping manoeuvrability of appropriate test fixtures at a manageable level. The size of the panels (length to thickness ratio) was also chosen to keep the behaviour of the structure to that of a plate i.e. allow for typical bending response to occur. Typical aspect ratios of 6:1 ensure this, although as this reduces below 3:1, the amount of flexure experienced by the target becomes negligible. Given these targets are meant to simulate face-sheet material, bending is of greater interest than purely through-thickness stresses, which would dominate in a target of low aspect ratio. Sandwich materials were provided by SP Gurit manufactured by P.E. Composites. The comparison of GFRP-skinned and CFRP-skinned sandwich materials and the steel plate was only performed for the explosive air blast experiments. Only GFRP materials were employed for the underwater blast experiments.

The composite tube construction was 40 mm inner diameter, 44 mm outer diameter made from 8 H Satin weave 300 g/m^2 (excluding CYCOM[®] 919 epoxy resin impregnation) known as weave style US 7781. The tube was constructed from 9 plies of 7781 epoxy rubber toughened thermoset E-glass fabric. The fabric weave style was selected as the mechanical properties are similar in both the warp and weft directions, simplifying the construction process. The exposed target length was 0.3 m. This size of target was chosen to allow for both the cross-sectional/circumferential and axial (bending) deformation to be observed. Tubular laminates were sourced from Tri-Cast. Table 1 shows a summary of the material properties provided by the manufacturer.

Table 1 Summary of materials used in the GFRP & CFRP sandwich panels and tubular laminates

Material	QE1200	RC245T	RC380T	P800	M130	CYCOM 919-7781
Density (kg/m ³)	1,750	1,390	1,390	155	140	1,320
Tensile modulus (GPa)	17	49	11	0.14	0.084	27
Compressive modulus (GPa)	–	–	–	0.13	0.13	29
Tensile strength (MPa)	250	470	–	–	–	470
Compressive strength (MPa)	200	310	–	2.8	–	480
Shear modulus (MPa)	6,500	3,100	23,600	61	49	–
Tensile failure strain (%)	≥1.5	–	–	–	–	≥1.7

3 Experimental

3.1 Air Blast Loading of GFRP- and CFRP-Skinned Sandwich Panels

Six different sample configurations were evaluated. Five of the targets were sandwich composite panels with lay-ups, shown schematically in Fig. 1. One panel is made of mild steel. There were two sets of samples tested for two different investigations. One set focussed on the influence of core thickness on panel response to air blast as well as the effect of different stand-off of the air blasts on the panel response (Series A). The second set focussed on the influence of skin type on the sandwich panel response to air blast (Series B).

GFRP-skinned and CFRP-skinned sandwich panels were subject to full-scale air-blast loading to observe the deformation and damage development with typical marine constructions. An overview of the test configurations is shown in Fig. 2 (see Fig. 2a for air blast studies). Full-field displacement plots of the back face of the target were obtained for the duration of the blast event by employing high-speed photography in conjunction with digital image correlation (DIC) methods. Two high-speed video cameras (Photron SA3s) were positioned behind the 1.6 × 1.3 m speckled targets and sampled at 2,000 frames/s at full resolution (1,024 × 1,024 pixels). This sampling frequency, required to suitably capture the event, was decided using a single degree of freedom model based on the procedure outlined by Biggs [29]. The time taken to reach maximum deflection for an air blast with say 2 bar peak shock pressure was established for each target to be within the region of 5 ms. Therefore by using the Photron SA3 cameras it was possible to operate at full resolution (keeping spatial resolution high), whilst capturing the images at a suitable rate (temporal resolution) for the DIC analysis to be conducted. These cameras were calibrated prior to testing to allow the recorded images to be processed in ARAMIS (produced by GOM mbH), the DIC software used to perform the image correlation calculations. A laser gauge was positioned on a steel beam mount as a secondary point measurement tool focussing on the centre of the panel, which sampled at

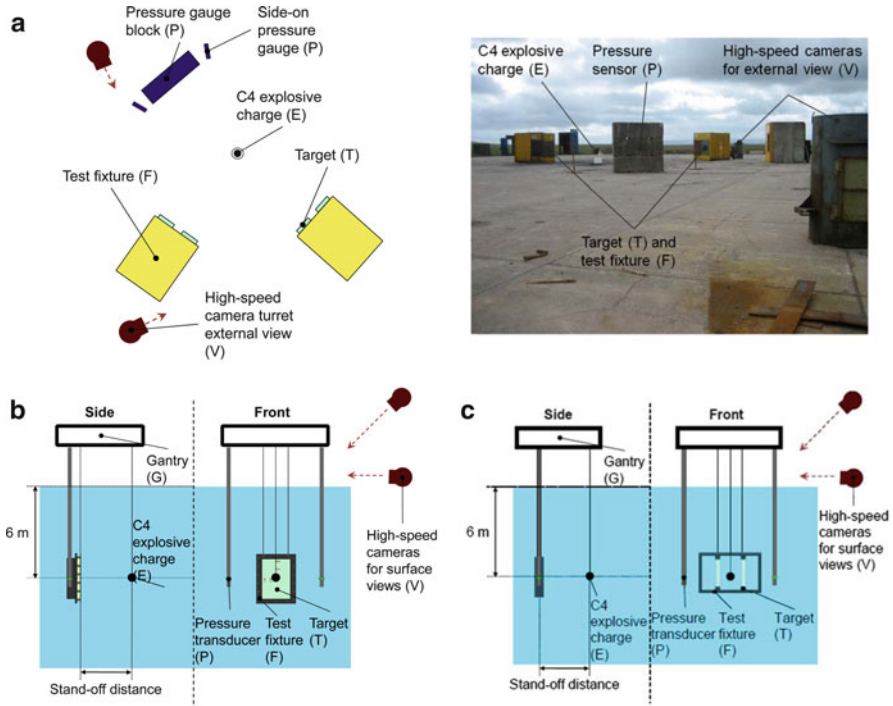


Fig. 2 Blast configurations showing schematic diagrams and images of the test set-up: (a) Air blast, (b) underwater blast of sandwich panels and (c) underwater blast of composite tubes. Featured in each diagram are: targets to be tested (T), sample fixtures (F), high-speed cameras and their relative locations (V), pressure sensor arrangements (P), gantry for the underwater tests (G) and C4 explosive charge (E)

2,000 Hz. The purpose of the laser gauge was to verify the results taken from the high-speed video recordings. Instrumentation is shown in Fig. 3 with the DIC set-up and laser gauge arrangement featured in Fig. 3a.

3.2 Air Blast Test Design and Other Instrumentation

Reflected pressure and static (side-on) pressure measurements were taken at the same stand-off distance from the charge as the target. High-speed video cameras were also positioned externally on the test pad, shielded in turrets, to capture front-face deformation as shown in Fig. 2a. For Series A, three GFRP-skinned targets were tested; two with a 40 mm thick core (denoted G1), one with a 30 mm core (denoted G2). The blast parameters used during the tests shown here were 30 kg C4 charge at a stand-off distance of 8 m and 14 m. The tests conducted at a 14 m stand-off distance (an equivalent peak shock pressure of approximately 2 bar) were

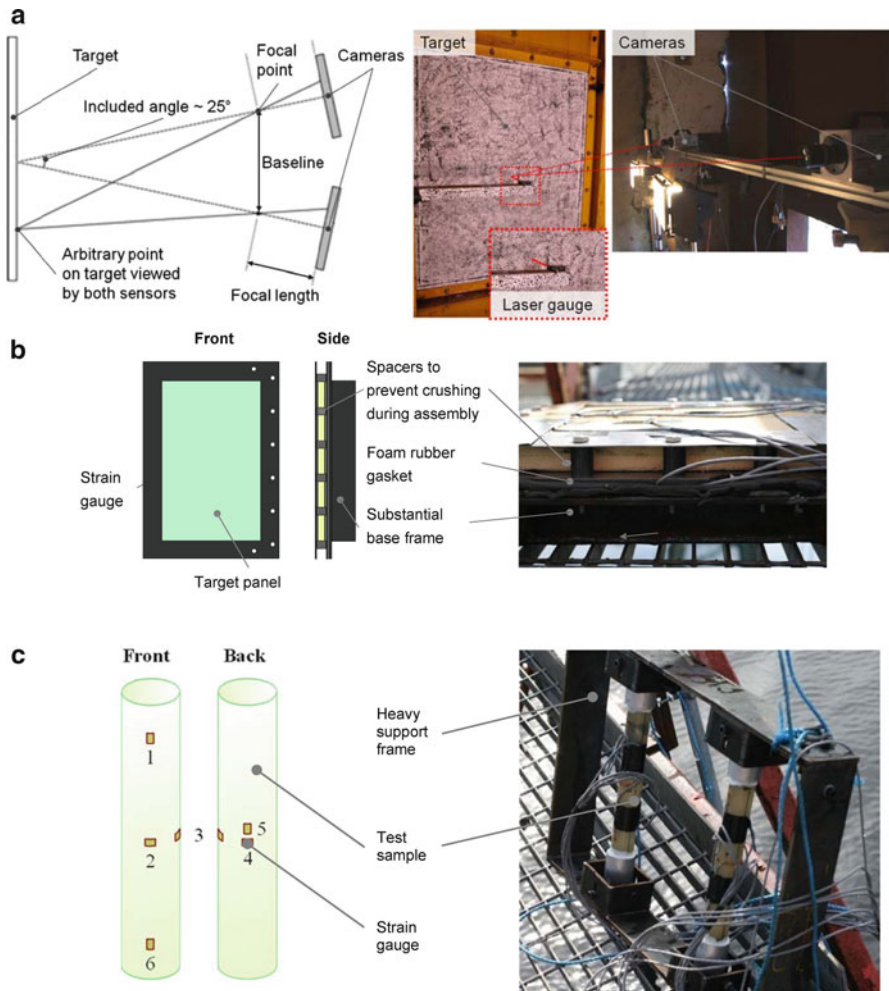


Fig. 3 Instrumentation: (a) Air blast featuring the DIC set-up and position of laser gauge; (b) Strain gauge arrangement for underwater blast loading of sandwich panels; (c) composite tubes

designed to take the panels to their elastic limit. The blast of 30 kg C4 at 8 m stand-off on G1 was designed to inflict damage on the target. For Series B, where skin comparison studies were conducted, one GFRP-skinned panel (denoted G3 with 25 mm core), one CFRP-skinned panel (denoted C1 with 25 mm core) and one steel plate (denoted S1) were evaluated. The blast parameters used during the tests shown here were 100 kg charges of Nitromethane (100 kg TNT equivalent) at a stand-off distance 14 m as this reduced stand-off correlated to the equivalent impulse which saw significant damage initiate in testing on Series A. FE simulations were conducted in ABAQUS to design the panel geometries, predicting the central peak deflections and peak surface strains below failure conditions (see Table 1).

3.3 Underwater Blast Loading of GFRP Sandwich Panels

GFRP sandwich panels were subject to underwater-blast loading to observe the deformation of the targets during the blast and damage sustained. A comparison can be made between the air and underwater blast cases as to differences in behaviour. Surface strain measurements were taken during the blast event using strain gauges positioned at 12 different locations. They were positioned along centre-lines of the panel face: three on the horizontal spaced evenly at 60 mm intervals from the centre and three on the vertical spaced evenly at 80 mm intervals 10 mm from the centre to avoid overlap of gauges. The other six gauges were positioned behind these locations on the rear face (shown in Fig. 3b). The strain gauges (and data acquisition hardware) chosen for this application was chosen specifically with the ability to monitor dynamic events (in terms of strain magnitude and strain rate). Once the gauges were bonded they were sealed in accordance to recommendations from engineers at Vishay Micro-Measurements to insulate from the environment and protect during impact, whilst maintaining a low profile and mass [30].

The panels were first bonded into a steel frame (3 mm thick mild steel). They were then bolted into a substantial base frame, comprising 10 mm thick mild steel, prior to testing. The base frame was designed to mitigate the effects of the blast wave wrapping around the target and interfering with its response to the incident wave acting on the front face. It also provided an enclosed volume behind the back-face of the panel to hold either air or water, which represents the conditions existing in a significant portion of a naval vessel. Thirdly it provided a weighty structure on its edges to replicate the boundary conditions experienced by a similar panel on the hull of a ship (from the support framework). A rubber foam gasket was used to create a seal for the backing fluid and to minimise the damage caused to the cables connected to the strain gauges on the rear face. Steel tube spacers were used to avoid crushing of the core material of the test panels, when bolted into the heavy base frame.

3.4 Underwater Blast Loading of GFRP Tubular Laminates

GFRP tubes were subject to underwater blast loads to assess how a tubular structure, a curved geometry, responds to such loads. Eight tubes were tested, seven filled and sealed with air inside (AF) and one with water (WF). One set of AF and WF tubes were paired to investigate the effect of the filling medium on the response of the tubes. The remainder of the air-filled tubes were tested in pairs and subjected to progressively increasing shock pressures to observe the damage inflicted on such constructions over a range of shock pressures. The sites thought to experience high principal stress during loading are at the ends of each tube on the front face (aligned square-on to the shock) and in the centre on the back face (this was also observed by [31] during similar aluminium shell trials). The two main motions observed during

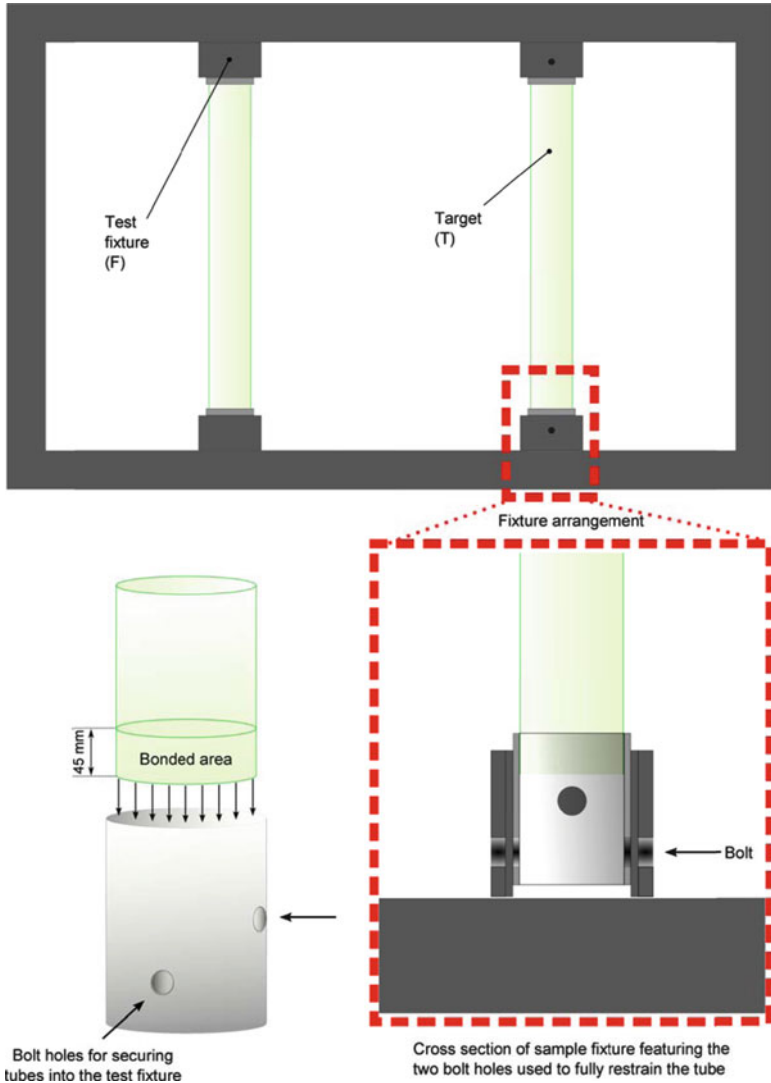


Fig. 4 Schematic of the assembly process of the test samples and the method used to attach the cylindrical samples in the test fixture

an underwater blast, bending and, what is commonly termed, breathing. These were deemed to be best observed by positioning three gauges axially, one at either end on the front and one at the centre on the back face, and three gauges circumferentially at the centre of the tube at 90° intervals (shown in Fig. 3c). The tubes were bonded into aluminium end-tabs and then bolted into a heavy steel frame, restraining the tube ends in all six degrees of freedom. This arrangement is shown in Fig. 4.

3.5 *Underwater Blast Test Design and Other Instrumentation*

High-speed video cameras were positioned on the test pad to capture the surface waves and disturbances during the blast from several angles. Static (side-on) pressure measurements were taken either side of the target using Neptune Sonar shock gauges. These were mounted on steel scaffold poles and lowered to the mid-height of the target. Details of the set-up are shown in Fig. 2b,c. Two panel targets were tested, one a 30 mm thick core (denoted G4) with air as the supporting fluid on the rear face and the other a 15 mm thick core (denoted G5) with water the supporting fluid. Blast parameters for the panel tests were 1 kg C4 charge at 6 m depth and a stand-off distance of 1.0 and 1.4 m respectively. These blasts were designed to cause significant damage to the targets to observe any trends regarding effects of backing fluid and differences between air-shock and underwater-shock regimes. The tubes were subject to a range of blast parameters, which involved using 0.5–1.0 kg C4 charges over a range of stand-off distances from 1.0 to 2.0 m at a 6 m depth. The details for specific tests will be mentioned alongside the results. The intention here was to also inflict significant damage to the tube structures, specifically, to observe progressive levels of damage in the air-filled tubes and highlight any effects of the filling medium on the observed response.

All positions of targets, charge and pressure sensors were verified using a submarine camera, prior to testing featured in Fig. 2b,c.

4 Results

4.1 *Air Blast of GFRP-Skinned and CFRP-Skinned Sandwich Composite Panels*

For Series A, two targets (G1 – GFRP-skinned with 40 mm core and G2 -GFRP-skinned with 30 mm core) were both initially subject to the same explosive charge (30 kg of C4) at the same stand-off distance (14 m). Figure 5 shows sample images taken from the high-speed videos positioned on the test pad. The shock wave is seen to arrive at the target 20 ms after detonation. This blast experiment was designed to take the panels to their elastic limit as stated in the Sect. 3.1. Figure 5 shows the test sample, with an arbitrary grid painted across it to enable ease of tracking the front-face deformation, held on the right-hand side in the test fixture (the large yellow cubicle, with the second window on the left-hand side of the fixture blanked out with a steel plate).

Figures 6 and 7 give a direct comparison between the target sandwich panels, G1 (40 mm core) and target G2 (30 mm core) respectively, with regard to their response to a given air-blast load. It can be seen that increasing the core thickness lowers the amplitude of oscillations. This is due to the increased stiffness of the plate, resulting from the increased core thickness.

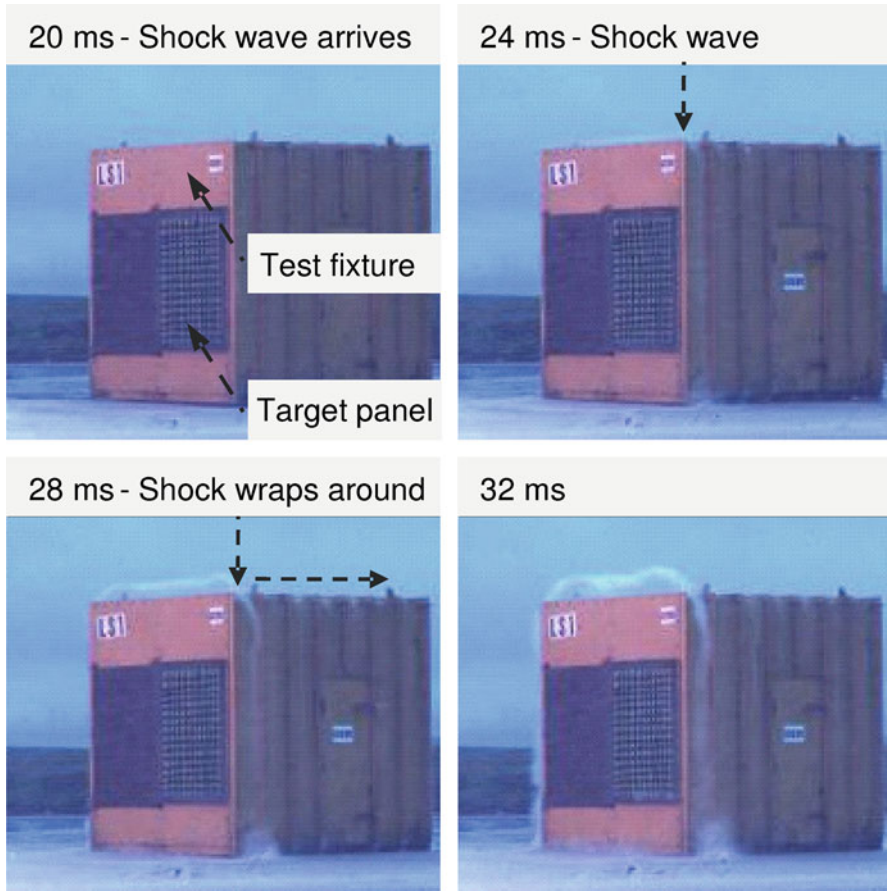


Fig. 5 Images of the shock wave impinging on the test sample (at 20 ms) and wrapping around the test cubicle thereafter (sandwich panel G1 with core thickness 40 mm and charge of 30 kg charge at stand-off of 14 m)

Figure 6 shows the central point deflection of G1 subjected to a recorded peak pressure of 2 bar (30 kg of C4 at stand-off of 14 m). The computed results from the image correlation are shown in the form of contour plots of out-of-plane displacement, principal strain and shear strain for the various times highlighted. It can be seen that the line from the left hand edge to the centre in the contour plots is the region of the specimen obscured by the laser gauge and its mount. This was employed to give an independent measure of central displacement in addition to DIC data. G1 was seen to deflect to a maximum distance out-of-plane of 63 mm (whilst Fig. 6 shows G2 deflected 78 mm). These deflection measurements agreed well with the laser gauge measurements for this single (central) point data, details to be discussed later in Sect. 5.1. The level of major principal strain peaked in the

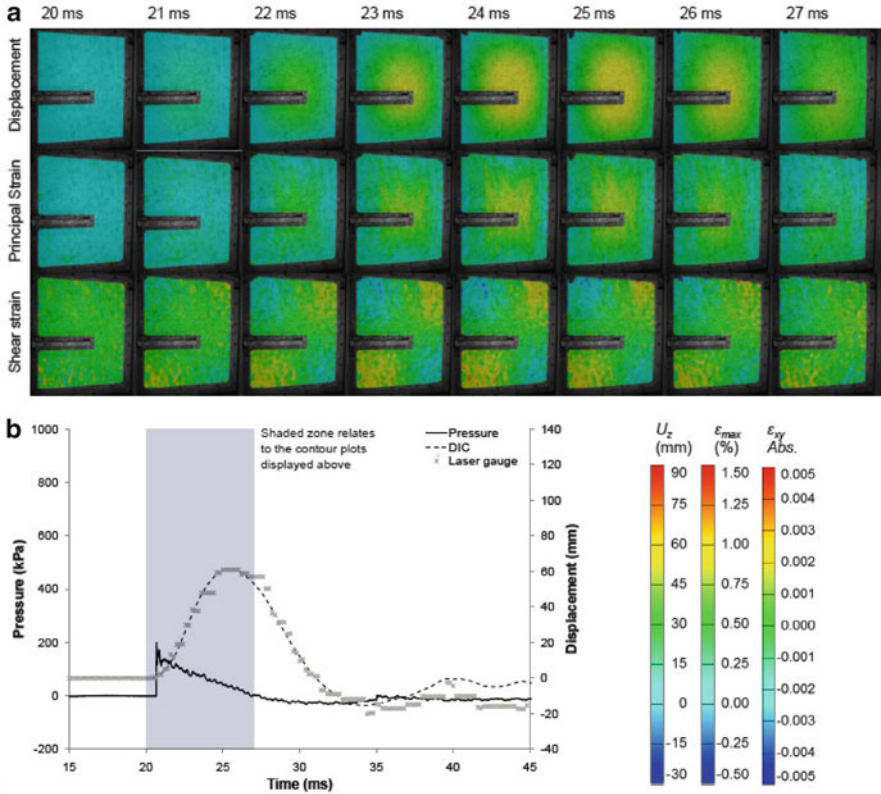


Fig. 6 Blast summary for 30 kg C4 at 14 m stand-off from G1 including: (a) DIC analysis and (b) a plot of pressure–time and displacement–time using both DIC and laser gauge centre point measurements. The DIC analyses features contour plots of out-of-plane displacement, maximum principal strain and shear strain, corresponding to various stages in the graphical plot. *The horizontal bar* visible in the contour plots (from the *left hand edge* to the *centre*) is the region of the specimen obscured by the laser gauge

region of 1% on the back face for G1. The G1 panel was deformed within a limit such that no visible damage was sustained. There were no obvious signs of damage shown within the DIC analysis for G1.

A similar response was exhibited in Fig. 7 for G2 with its reduced core thickness when subjected to a recorded peak pressure of 2 bar (30 kg of C4 at stand-off of 14 m). For G2, surface strains peaked at 1.25% and below the expected failure strains of the fibres. The lower limit (assuming a linear elastic relationship) for fibre strain to failure is 1.4% (as stated in Table 1). Signs were, however, observed within the DIC analysis that mild sub-surface core cracking had occurred. Early discontinuities in the major principal strain plots indicate possible detachment of the skin from the core i.e. possible cracking. This was confirmed upon sectioning of the panel after the blast.

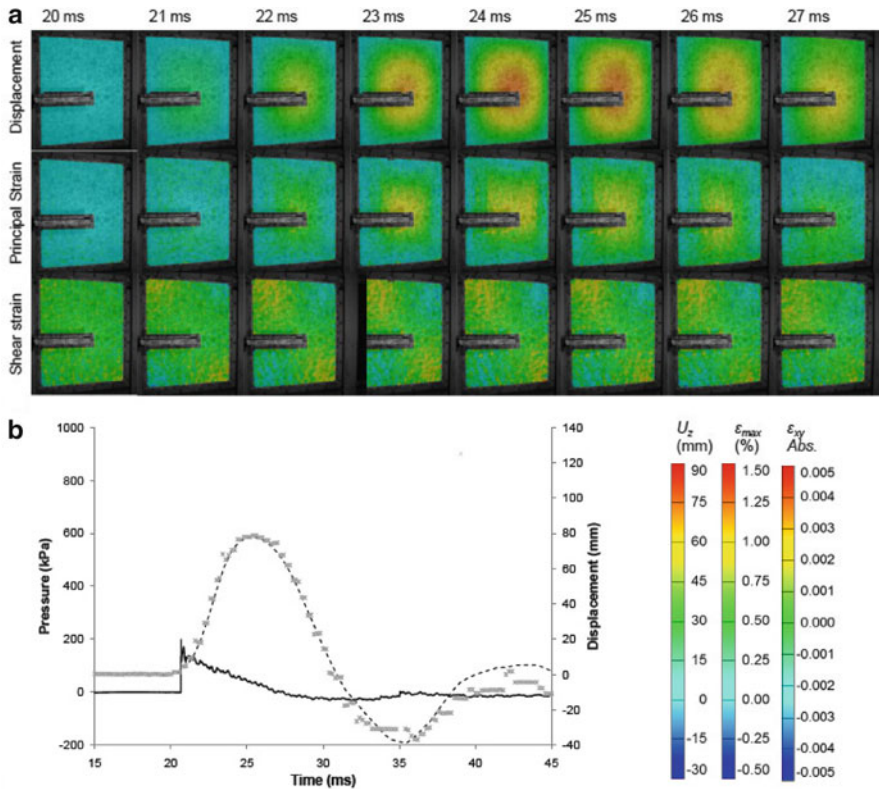


Fig. 7 Blast summary for 30 kg C4 at 14 m stand-off from G2 including: (a) DIC analysis and (b) a plot of pressure–time and displacement–time using both DIC and laser gauge centre point measurements. The DIC analyses features contour plots of out-of-plane displacement, maximum principal strain and shear strain, corresponding to various stages in the graphical plot. *The horizontal bar visible in the contour plots (from the left hand edge to the centre) is the region of the specimen obscured by the laser gauge*

As the DIC analysis agreed with predictions for peak elastic displacements of the targets due to a 2 bar shock pressure, and both the DIC analysis and visual inspection showed no visible skin damage to panel G1, it was decided that another panel of the same construction as G1 be subject to a more substantial blast to induce significant skin and core damage. This highlighted clearly the failure diagnostic capabilities of the DIC technique in this context. Blast parameters for this final air blast involved a 30 kg charge positioned at a reduced stand-off of 8 m from G1. Figure 8 shows the progressive deformation and eventual skin damage inflicted on G1 by the 8 bar pressure shock wave. A skin crack is seen to originate from the top left hand edge of the panel and propagate down that side of the target.

Figure 9 shows the measured reflected pressure as well as the central out-of-plane displacement during the blast event for G1 (GFRP-skinned with 40 mm core)

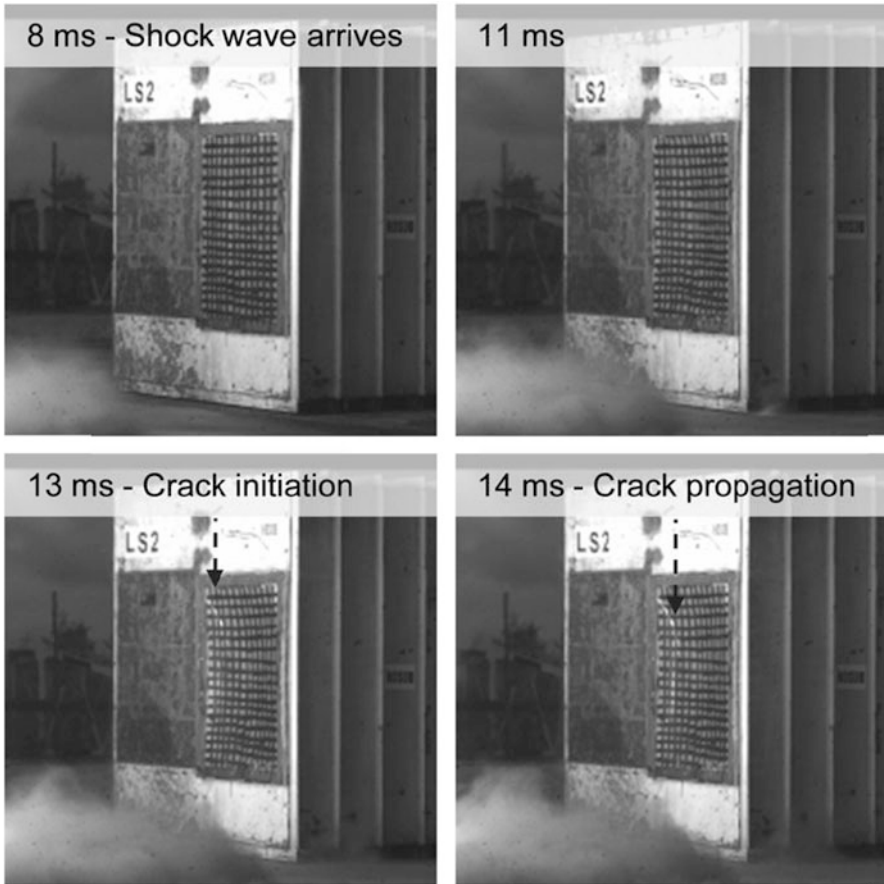


Fig. 8 Images of the shock wave impinging on the test sample (8 ms) causing deformation and front-skin damage thereafter (sandwich panel G1 with core thickness 40 mm and charge of 30 kg charge at stand-off of 8 m)

with at 30 kg charge at stand-off of 8 m. Comparing this plot of out-of-plane displacement to that shown earlier in Fig. 6, besides from the magnitude of peak out-of-plane displacement, immediately one can notice the difference in smoothness of the path taken during the first oscillation. Looking closely at the time period 12.5–13.5 ms, one can observe a flattening in the displacement curve near its maximum condition. This coincides with the time (13 ms) when the crack is observed to form in Fig. 8.

The peak out-of-plane displacement was 131 mm and strains peaked in the region of 3% prior to the crack developing. Upon post inspection, the front face sustained inter-laminar skin failure and front-ply fibre breakage whilst the core suffered a severe skin-to-skin crack (see Fig. 10). Towards the centre of the panel, the severity of the failure increased.

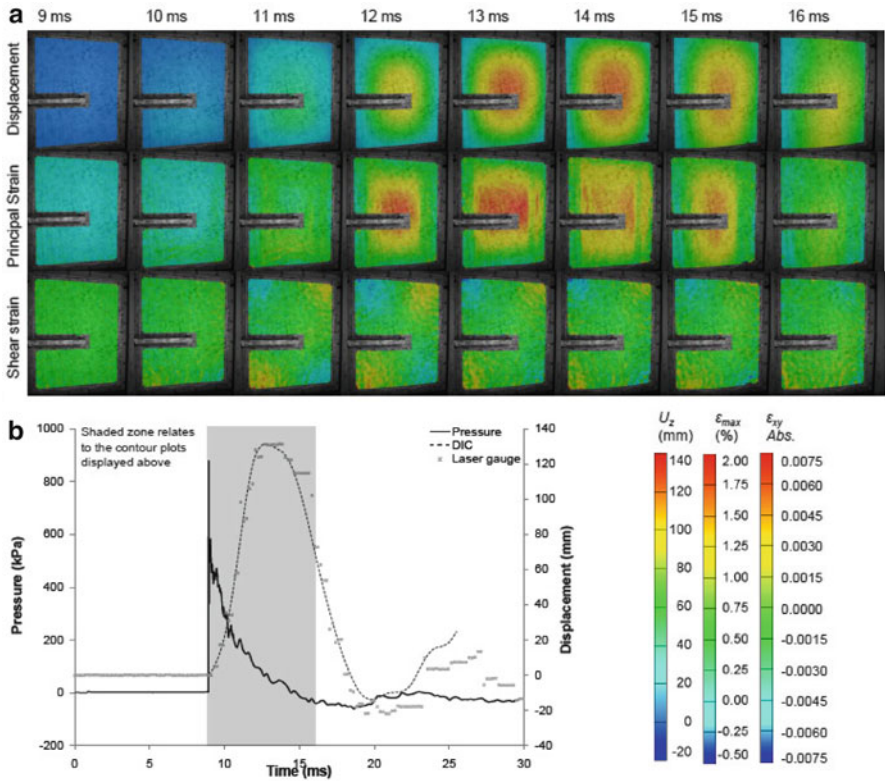


Fig. 9 Blast summary for 30 kg C4 at 8 m stand-off from G1 including: (a) DIC analysis and (b) a plot of pressure–time and displacement–time using both DIC and laser gauge centre point measurements. The DIC analyses features contour plots of out-of-plane displacement, maximum principal principal strain and shear strain, corresponding to various stages in the graphical plot. The horizontal bar visible in the contour plots (from the *left hand edge* to the *centre*) is the region of the specimen obscured by the laser gauge

For the series B experiments, glass-skinned and carbon-skinned sandwich panels were compared: G3 (GFRP-skinned with 25 mm core) and C1 (CFRP-skinned with 25 mm core). The air blast employed 100 kg charge Nitromethane at 14 m stand-off. The samples were tested side-by-side (in the same test fixture) to compare directly the response of the GFRP-skinned sandwich panel to the CFRP-skinned sandwich panels. The two types of panel had similar mass per unit area ($\sim 17 \text{ kg m}^{-2}$) with the constructions forming panels of the same thickness (same thickness of skins, 2 mm each, on the same thickness of core, 25 mm). The two types of panel provide a good comparison for observing the effect of skin configuration on blast mitigation. A sample of sheet steel (S1) was also tested under these conditions to provide a comparison against traditional naval engineering materials. Central point displacement, full-field contour DIC data and pressure data will be provided for the duration of the event.

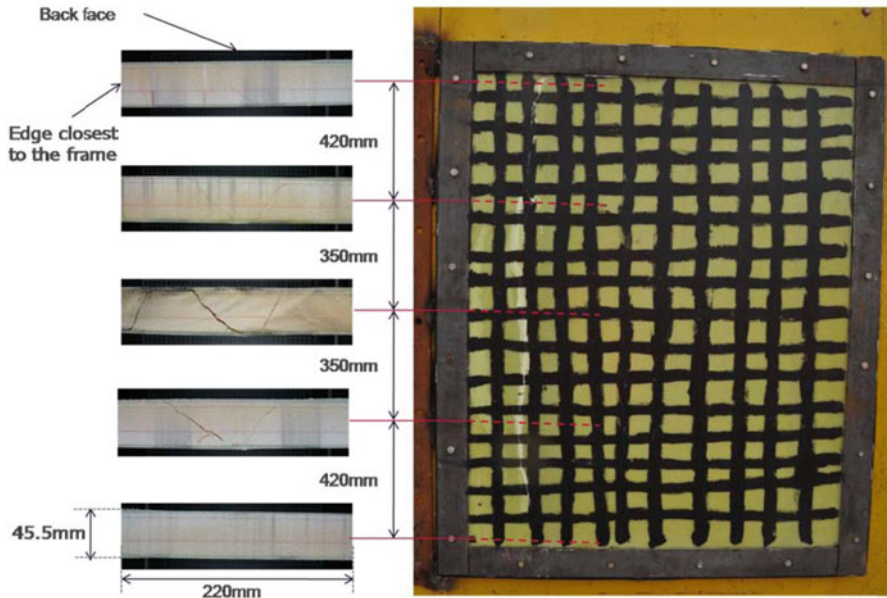


Fig. 10 Front face damage on G1: The whole panel with a clear crack down the *left-hand edge* of the panel (*right*), sectioned at regular intervals showing various failure mechanisms (*left*). This is for sandwich panel G1 – GFRP-skinned with core thickness 40 mm and charge of 30 kg charge at stand-off of 8 m

The 100 kg TNT at a 14 m stand-off blast was employed to give a severe comparison of CFRP-skinned composite sandwich panel (C1) with the GFRP-skinned composite sandwich panels (G3). The result for the experiment, forming the visible damage post-test, is presented below (for G3 and C1). Figure 11 shows the progressive deformation and eventual skin damage inflicted on the panel by the blast, where the peak overpressure was equal to 2.5 bar, corresponding to a 100 kg charge Nitromethane at 14 m stand-off. Unlike previous blast experiments, the overpressure or side-on pressure was measured rather than the reflected pressure. A skin crack is seen to originate from the top right hand edge of the panel at approximately 19 ms into the blast event and propagate down that side of the target.

Figure 12 shows a summary of the blast data recorded for G3 in this blast (100 kg Nitromethane at 14 m stand-off). From the graphical plot in this summary, around maximum out-of-plane displacement, the distortion (due to damage initiation and propagation) of the return stroke of the target is clear. Between the time period 19.0–22.0 ms, one can observe a flattening in the displacement curve around its maximum. This coincides with the time period over which the crack was observed to initiate and propagate in Fig. 11 from the top right-hand corner of the GFRP panel. Maximum deflection was found to be 140 mm and the strain peaked in the region of $\sim 1.6\%$ prior to the crack developing.

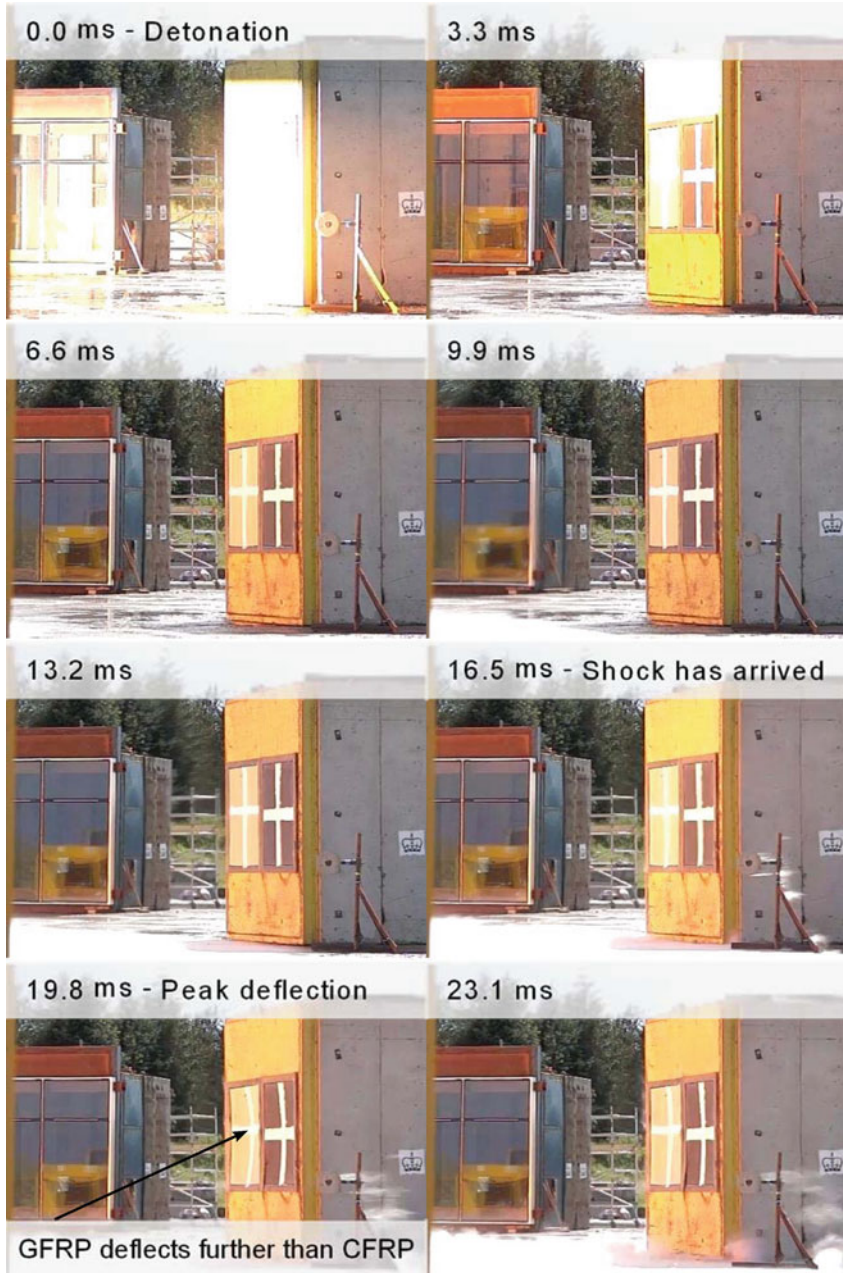


Fig. 11 Images of shock wave progression and front-face deformation of G3 and C1(GFRP-skinned sandwich panel G3 with core thickness 25 mm and CFRP-skinned sandwich panel C1 with core thickness 25 mm separately subject to 100 kg TNT equivalent charge at stand-off of 14 m). Images are shown from the detonation (0 ms) through the shock wave arrival at target (15 ms) until targets begin their first rebound. Exact time at which these event occur are not shown in the images (due to availability), therefore timings of interest are highlighted around those exact times

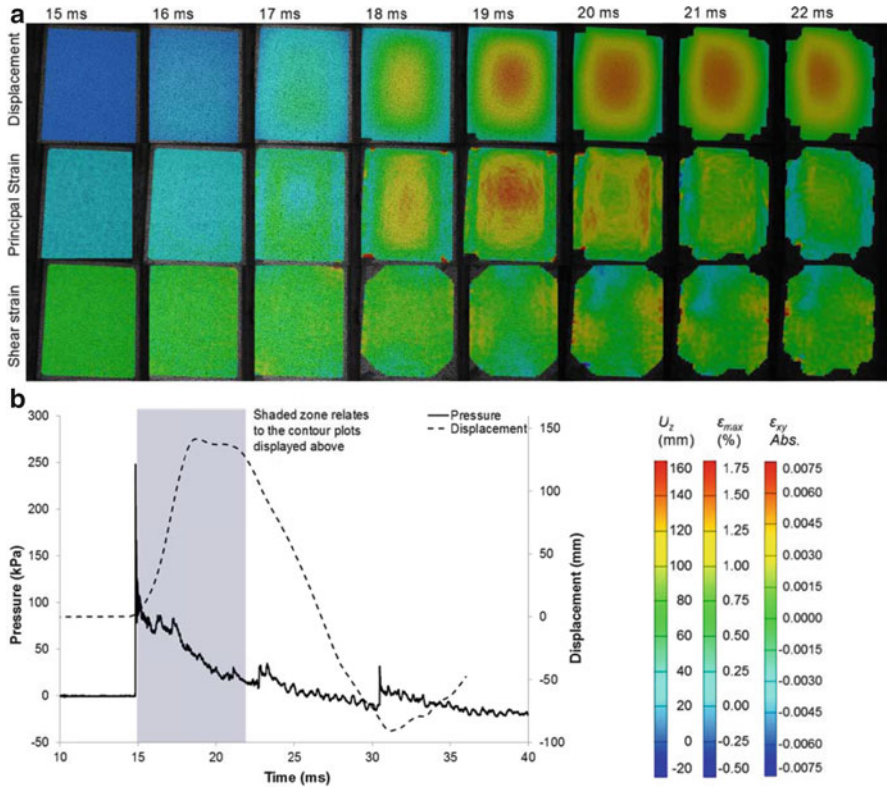


Fig. 12 Blast summary for 100 kg TNT equivalent at 14 m stand-off from G3 including: (a) DIC analyses and (b) a plot of pressure–time and displacement–time using both DIC and laser gauge centre point measurements. The DIC analyses features contour plots of out-of-plane displacement, maximum principal strain and shear strain, corresponding to various stages in the graphical plot

Comparatively C1, in Fig. 11, is observed to deflect noticeably less than G3. The two panels are subject to the same blast (recorded peak pressure of 2.5 bar and duration ca. 12 ms). There are of course asymmetry effects with regard to the load distribution, however in this case the support structure is completely symmetrical and the charge was positioned central to the test structure, therefore any asymmetry of loading can be assumed to be consistent for both targets. A considerable skin crack is seen to form in G3, however C1 formed no global failure similar to G3. A fine crack was observed to form towards one of the panel edges and the core shear failure was still observed to a similar severity as for G3. Figure 13 shows a summary of the blast data recorded for this blast (100 kg Nitromethane at 14 m stand-off). The carbon-skinned sandwich panel (C1) exhibits a greater resistance to the blast than glass-skinned sandwich panel (G3). The stiffer carbon skins minimise maximum deflection to 107 mm (compared to 135 mm for G3). The contour plots in Fig. 13 show a larger central region than G3. This is perhaps because more of the blast energy was distributed throughout the structure in C1, causing less severe but

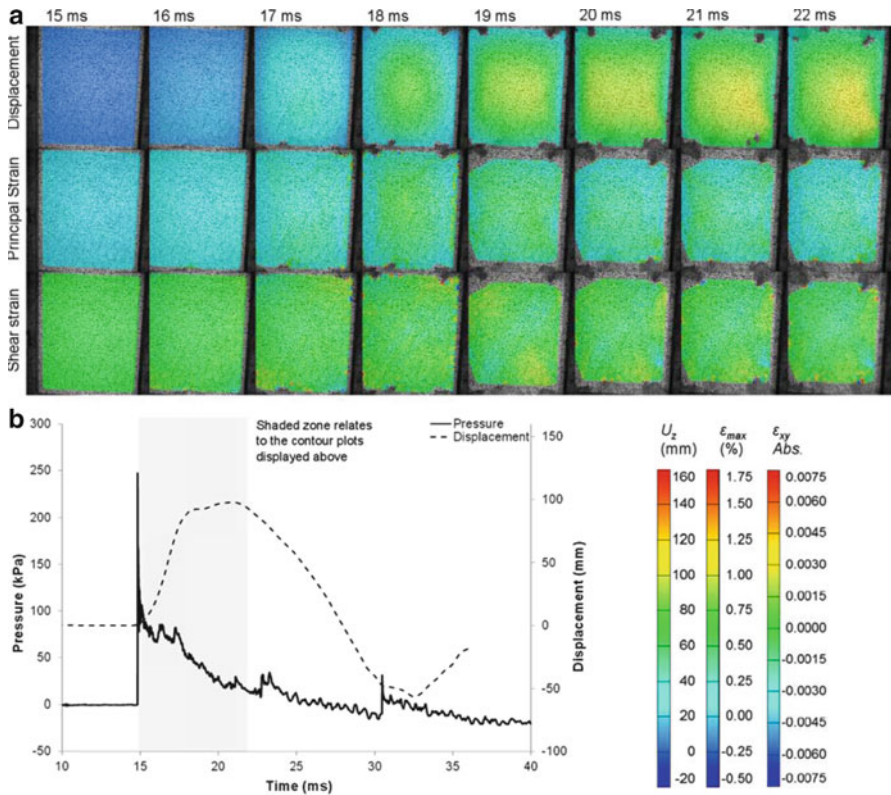


Fig. 13 Blast summary for 100 kg TNT equivalent at 14 m stand-off from C1 including: (a) DIC analyses and (b) a plot of pressure–time and displacement–time using both DIC and laser gauge centre point measurements. The DIC analyses features contour plots of out-of-plane displacement, maximum principal strain and shear strain, corresponding to various stages in the graphical plot

more widespread core cracking. Conversely G3 did not distribute the blast energy quick enough throughout the entire structure leading to a major localised failure of the skin and core. This type of damage mechanism (core cracking) accounts for the elongated return of C1 observed in Fig. 13. The time taken for the panel to return to its original position took an extra millisecond in the carbon panel compared to the glass panel. This extended response time absorbed the blast energy over a longer time period, resulting in a lower observed maximum deflection (107 mm) and maximum strain ($\sim 0.8\%$) compared to G3.

Upon post inspection, the front face sustained inter-laminar skin failure and severe front-ply fibre breakage whilst the core suffered cracking from skin to skin but the rear skin remained intact. Figure 14a shows an overview of the damage observed by the two panels. The front skins were more severely damaged in the GFRP-skinned composite sandwich panels (G3). This is when compared to the CFRP-skinned sandwich panels (C1). For both panels the rear skins of the composite sandwich panel showed no visible damage. This was consistent with



Fig. 14 (a) Before and after images taken of the front face view of G3 and C1 after being subject to a charge of 100 kg TNT equivalent at stand-off of 14 m. (b) Images featuring the damage sustained by G3 and C1 after being blasted

previous air blast experiments in Series A. There was core damage present in G3 and C1 resulting from front skin failure and interlaminar failure between front skin and core. This damage initiated for G3 in transition regions from constraint to regions of deflection of the panel. This is where the stress state caused by the restraint and the impulsive loading, promotes failure initiation. The lack of sufficient distribution of energy lead to global propagation of the crack in the GFRP panels compared to the CFRP panels, which have small areas of skin cracking (which actually probably initiated from the stress concentration at the bolt hole, see Fig. 14b).

The other blast conducted during this set of experiments involved a mild steel plate (S1) of a near equivalent mass per unit area ($\sim 23 \text{ kg/m}^2$) as per the GFRP and CFRP sandwich materials ($\sim 17 \text{ kg/m}^2$) tested. This steel sheet was used to illustrate clearly the differences that exist between conventional construction materials and the latest style of naval constructions. Figure 15 shows the external view captured of the deformation process. There are similarities, from first impressions of the nature of deformation observed in terms of shape for instance. However further analysis of this footage and analysis of the DIC data uncovers distinct differences. Figure 16 gives a summary in the same fashion as for G3 and C1. From the plot in Fig. 15b there is an almost linear initial portion of response, however at around 20 ms the panel pulls out from six bolt holes. This dissipates a lot of energy (and relieves the intensity of the oncoming pressure wave providing clearing for the blast wave too), hence the sharp decrease gradient of the displacement-time plot. The curve is then seen to decrease in gradient steadily until it reaches a plateau, where all the momentum has transferred to plastic deformation of the steel sheet.

The contour plots in Fig. 16 only show the deformation within the time period shown for that of G3 and C1. This shows that the panel deformed significantly more than the sandwich structures. Moreover S1 folded and crumpled in the regions between the bolt holes where high shear stresses causing this crumpling to occur.

S1 had a peak deflection which was 270 mm, which is considerable more than GFRP and CFRP skinned sandwich panels. A deflection of approximately 120 mm was attained prior to bolt shear, which dissipated some energy and also relieved some of the blast pressure. Major principal strain peaks at approximately 1.1%. The damage sustained by S1 is featured in Fig. 17, showing the final deformed profile relative to its original at profile.

4.2 Underwater Blast Loading of GFRP Sandwich Panels

Two sandwich panel targets, G4 (GFRP-skinned with 30 mm core thickness) and G5 (GFRP-skinned with 15 mm core thickness), were subject to two different blast scenarios. There were two different impulses and two different sets of boundary conditions to explore the effect of the backing (or supporting) medium to the target's response. A 1 kg C4 explosive charge was set at the mid-height of the target 6 m below the surface of the water at a stand-off distance of 1 m for G4 with an air-pocket encapsulated behind the target. G5 had the 1 kg charge of C5 1.4 m away at the same depth but this time with water encapsulated behind the target. Although only a 1 kg charge was used this was still substantial given the transition from air blasting to underwater.

Surface effects propagating from the blast event were recorded and sample images are shown in Fig. 18. The sequence runs through the initial shock producing a spray at the surface at about 5 ms, which remains until the bubble begins to rise, forming a dome at the surface after the first 1,000 ms. This reaches a peak height of approximately 1 m prior to venting at 1,400 ms, throwing a large mass of water up in the air.

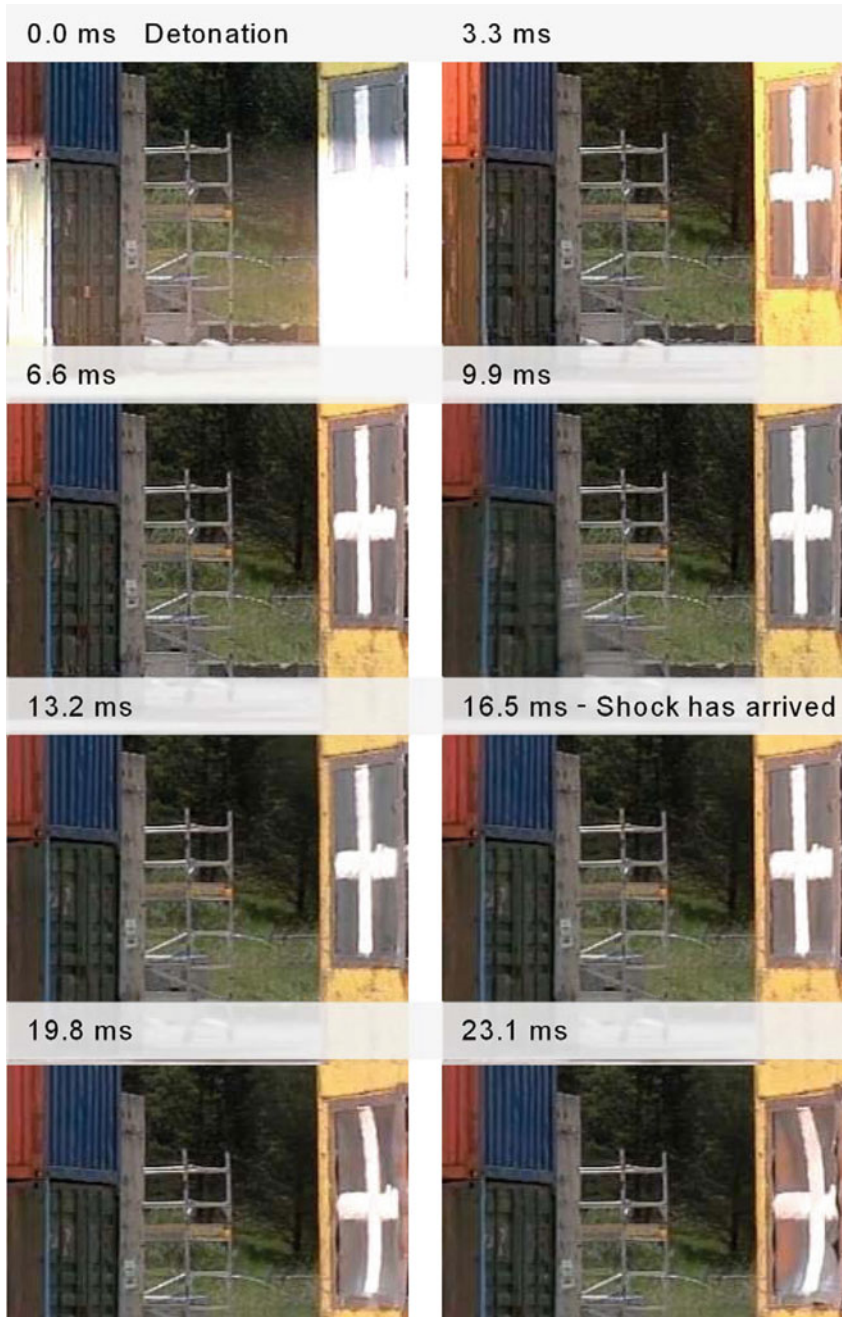


Fig. 15 Images of shock wave progression and front-face deformation of S1 (3 mm thick steel plate). Images are shown from the detonation (0 ms) through the shock wave arrival at target (15 ms) until targets begin their first rebound. Exact time at which these event occur are not shown in the images (due to availability), therefore timings of interest are highlighted around those exact times

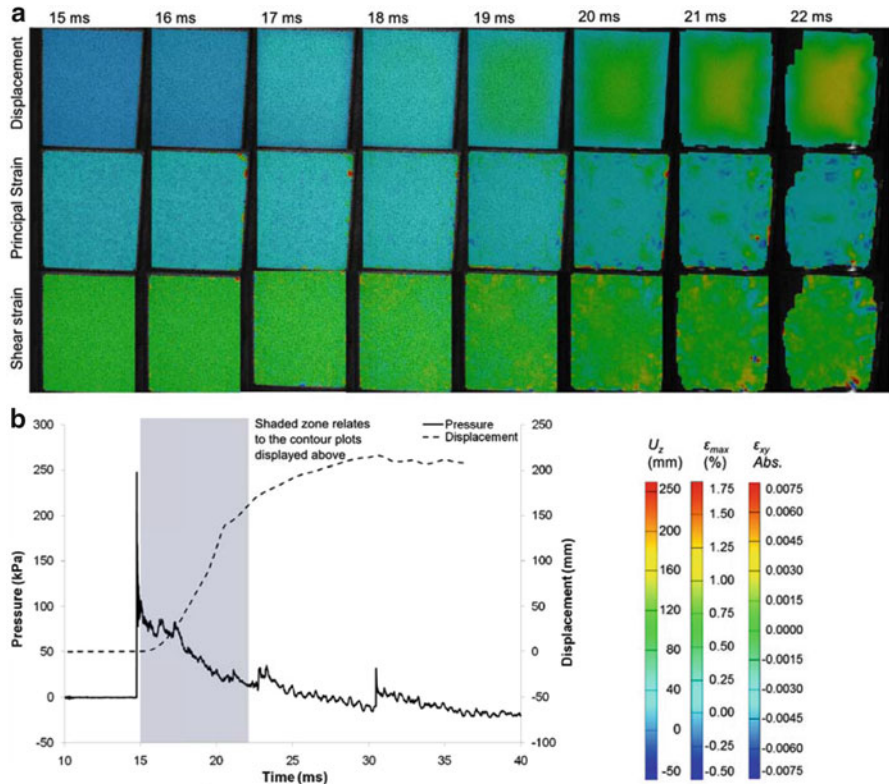


Fig. 16 Blast summary for 100 kg TNT equivalent at 14 m stand-off from S1 including: (a) DIC analyses and (b) a plot of pressure–time and displacement–time using both DIC and laser gauge centre point measurements. The DIC analyses features contour plots of out-of-plane displacement, maximum principal strain and shear strain, corresponding to various stages in the graphical plot

Blast pressures experienced by panels G4 (30 mm core) and G5 (15 mm core) peaked at a shock pressure of 430 bar (1 kg of C4; 6 m depth; stand-off 1 m; panel air-backed) and 300 bar (1 kg of C4; 6 m depth; stand-off 1.4 m; panel water-backed) respectively. The two pressure–time traces are shown in Fig. 19 for the two blast scenarios, illustrating the ferocity of the blast event, note that the strain gauge data will be restricted to the initial response also highlighted in Fig. 19. Figure 20 shows an example of all strain gauge data for G5. These pressures are very high shock pressures to subject the test panels to and it resulted in significant damage sustained by the targets. The air-backed G4 had its core crushed to half the original thickness (16 mm core thickness reduction) by the shock. There were initial surface strains in the region of 3% and once the panel membrane response began, surface strains of around 1% remained causing severe cracks to form within the skins along the panel edges. This is evident in Fig. 14.

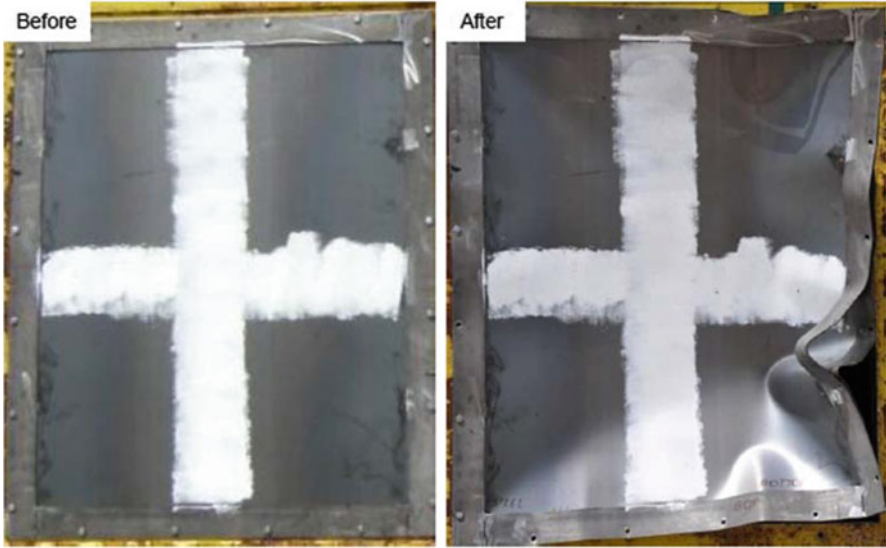


Fig. 17 Before and after images taken of the front face view of S1 after being subject to a charge of 100 kg TNT equivalent at stand-off of 14 m

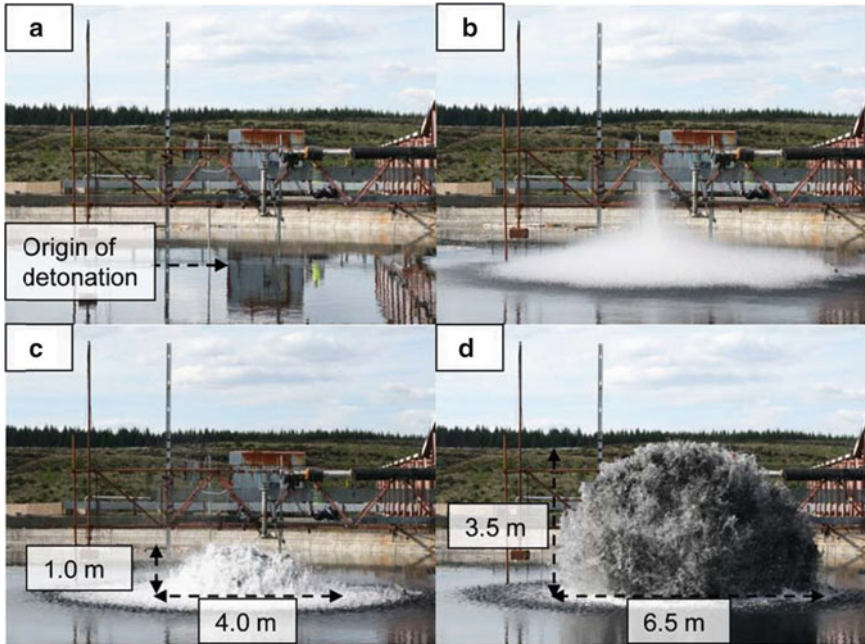


Fig. 18 Images of the event taken from the edge of the pond of the water surface. Different stages of the blast event are shown: (a) Prior to detonation with various aspects of the set-up highlighted; (b) Initial shock wave reaching the surface of the water causing a spray of water to form at the surface; (c) Bubble migrating upwards forming a dome on the surface of the water (at $\sim 1,000$ ms); (d) the bubble venting to the atmosphere throwing a mass of water into the air (at $\sim 1,400$ ms)

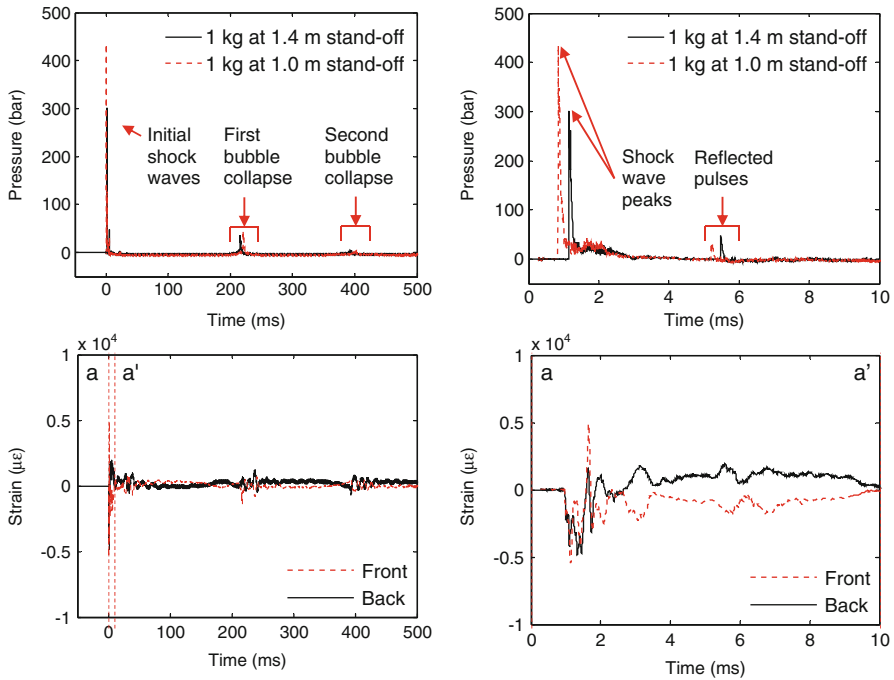


Fig. 19 Pressure–time traces for 1 kg blasts at stand-offs of 1.0 and 1.4 m: the entire event including the first bubble pulse at ~200 ms (*top left*); and initial shock pressure including reflected shock at ~5 ms (*top right*). Sample strain gauge data of the panel response is given over these time periods for strain gauge position 1 (as shown in Fig. 3), front and back face, of the water backed-panel G5 (15 mm core thickness) when subjected to the 1 kg charge C4 at 1.4 m stand-off

The water supporting the rear face of panel G5 was observed to dampen the overall response of the panel during the blast. The large strains observed in G4 were not observed in G5 due to the fact that the water medium supported the panel and restrained its response to the blast. Typical flexural response of the plate under a distributed transient pressure load was not observed. This is why surface strains generally remained low over the entire target area of G5 (water-backed) in comparison to the blast on G4 (air-backed), where strain magnitude rose towards the centre of the target. The fact that G5 experienced a decreased impulse was irrelevant; the change in the response characteristics is what has occurred. Figure 20 shows that strains peaked at $\pm 0.6\%$ on the front face and -0.6% on the back face of G5. Each face initially went into a state of compression, forcing the sandwich panel inwards on itself. After this, typical oscillatory motion ensued with strains of $\pm 0.2\%$ resulting. There was no visible damage to the skins after the blast; however, the 15 mm thick core suffered significant crushing as shown in Fig. 21c (7 mm core thickness reduction). This was again in the region of 50% core thickness reduction this time for a peak shock pressure of 300 bar (130 bar lower than that observed for G4) and an impulse of 4.82 bar ms (compared to 6.41 bar ms for G4). The

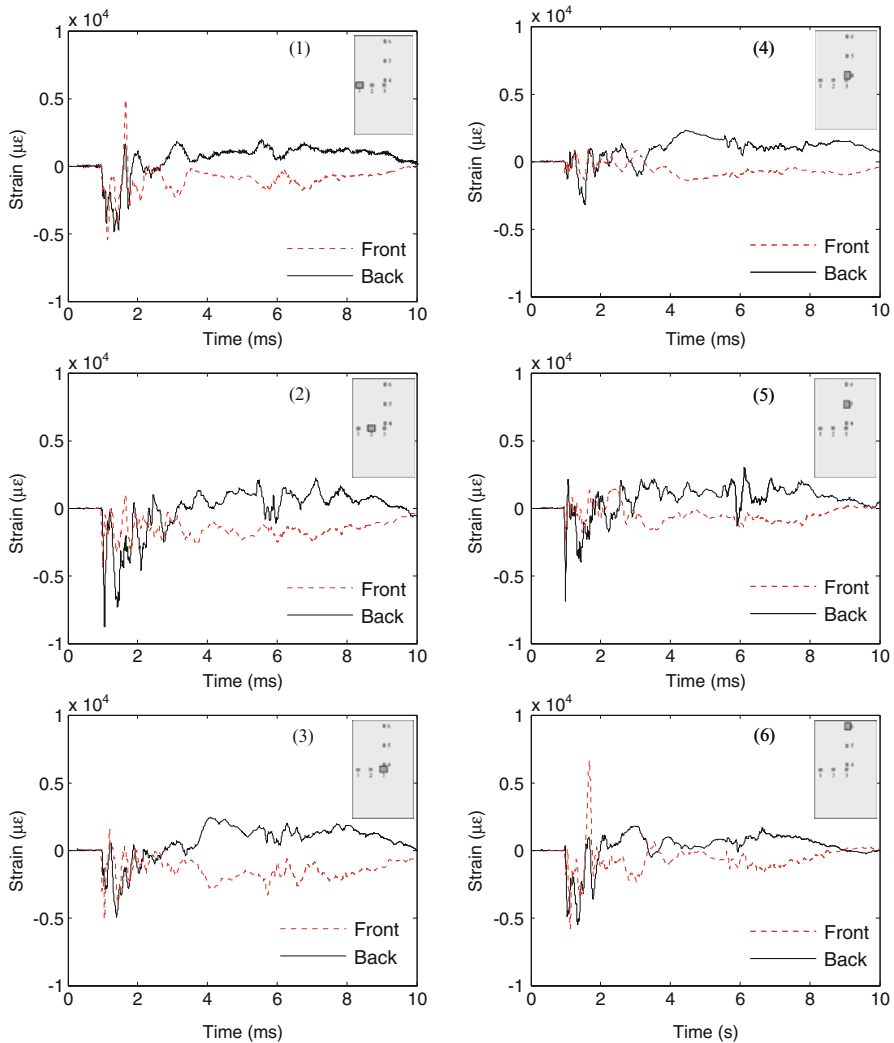


Fig. 20 Sample strain gauge data displayed for G5 (core thickness 15 mm) sandwich composite panel with water on the front and back face (300 bar; 1 kg of C4; 6 m depth; stand-off 1.4 m). Data is displayed for the first 10 ms for each gauge position (numbered as shown in Fig. 3)

two panel responses for G4 and G5 were compared in Fig. 21, the difference in strain magnitude is highlighted as well as the effect of the backing medium with the water-backed G5 (see Fig. 21a) experiencing lower surface strains compared to the air-backed G4 (see Fig. 21b). Moreover the characteristic response of a plate due to impulsive loads was captured by the strain gauge data for the air-backed G4 illustrated in Fig. 21c. The plate experienced an initial compression near the top edge of the panel whilst the central region remained in tension as evident in the strain gauge response shown in Fig. 21b.

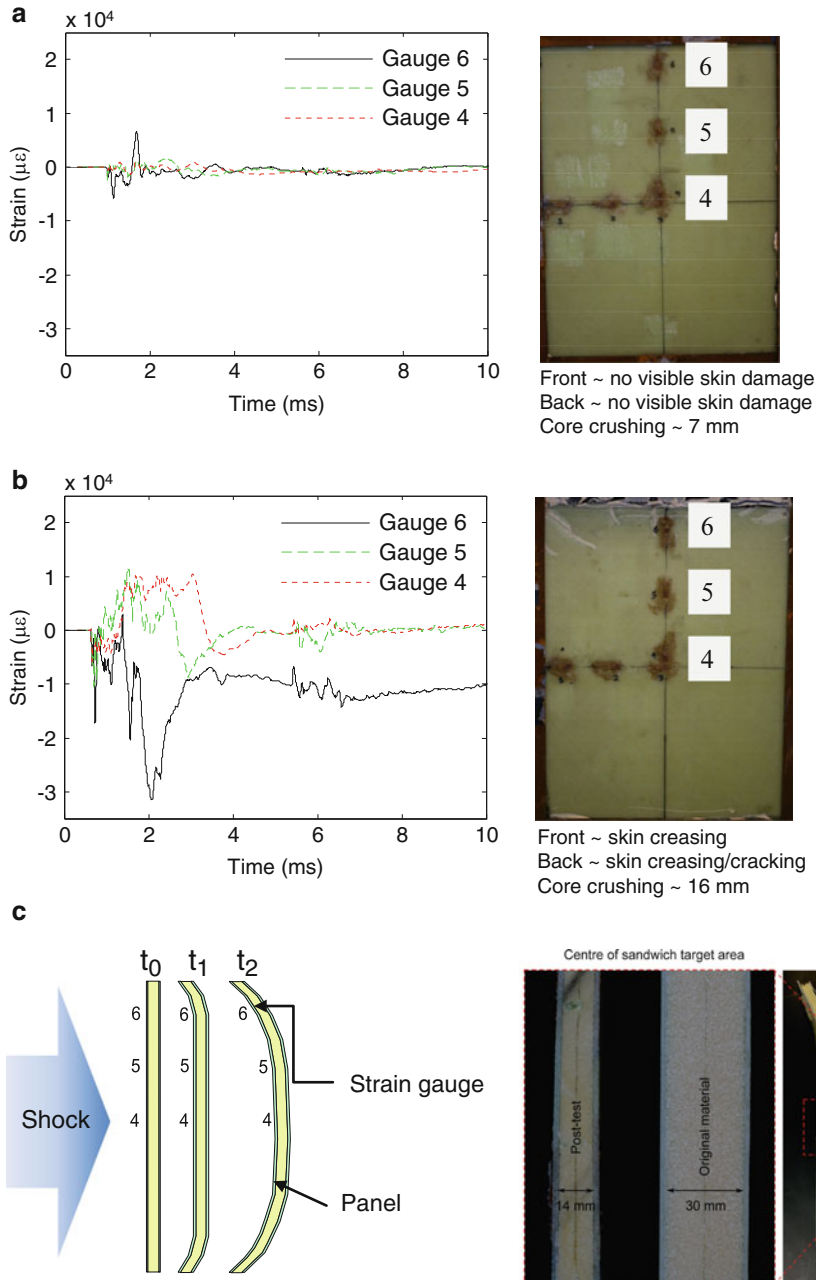


Fig. 21 Comparison of underwater blast response of sandwich panels tested: The first 10 ms of strain gauge data is displayed for gauge positions 4–6 (numbered as shown in Fig. 3) for: (a) water-backed sandwich panel G5 (core thickness 15 mm) with shock: 300 bar (1 kg of C4; 6 m depth; stand-off 1.4 m); (b) air-backed sandwich panel G4 (core thickness 30 mm) with shock: 430 bar (1 kg of C4; 6 m depth; stand-off 1.0 m); (c) diagrammatic representation and sectional views (before and after shock loading) of G4

4.3 Underwater Blast Loading of GFRP Tubular Laminates

4.3.1 Progressive Shock Loading of GFRP Tubular Laminates

Figure 22 shows the combined pressure time traces for each underwater blast on composite tubular laminates of air-filled (AF) design. Peak pressures ranged from 180 to 400 bar for a range of blast parameters from 0.5 kg C4 explosive charge at a 2.0 m stand-off distance at a 6 m depth to a 1.0 kg charge at 1.0 m stand-off distance at the same depth. Figure 16 shows the combined results for the progressive loading of these tubular laminates. The 180 bar blast produced no visible skin damage to the targets with the surface strains sufficiently low to form an agreement with this observation. The 240 bar blast proved to be the threshold for damage evolution with surface strains reaching 1%. The tubes were then tested at a peak shock pressure of 350 bar and visible damage was inflicted on the targets with axial cracks forming along the front facing side of the sample as strains reached 1.5%. In the final test the tubes were taken beyond their limit, where complete shear failure was observed for a peak shock pressure of 400 bar. Similar signs of axial cracking were observed in this final sample (as for the blast of 350 bar) evident from the remains at the end-tabs featured in Fig. 23 prior to the entire gauge length shearing off at the supports.

4.3.2 Effect of Filler Fluid on Tubular Laminate Response

One tube of each air filled (AF) and water filled (WF) design were subject to 350 bar peak shock load caused by a 1 kg C4 charge at 1.4 m stand-off at 6 m depth (pressure–time history shown previously in Fig. 22). There is the initial compression/collapse of the tube inwards at its centre prior to the oscillatory squashing motion. However when these traces in gauges 2–4 for AF are compared to WF (see Fig. 24), there is a marked difference in response. Using water as the filler fluid causes a damped the amplitude of response, reducing peak strains from 1.5% in AF to 0.5% in WF (see gauge position 4 recording the fluctuation in hoop strain on the back facing side of the tube in Fig. 24).

The tubes were both subject to a pressure of 350 bar (there were two independent recordings of pressure either side of the targets). The damage sustained by AF relative to WF was apparent with no visible damage observed for WF whereas AF shown in Fig. 25 shows axial cracking, most likely caused by shear failure during the circumferential crushing phase of the sample deformation causing cracks to initiate.

5 Discussion and Analysis

These sandwich composite structures, although very simple in construction, provided significant blast resistance to shock loading. They sustained a pressure loading of 2 bar in air without resulting in a catastrophic failure. The back face of the panel

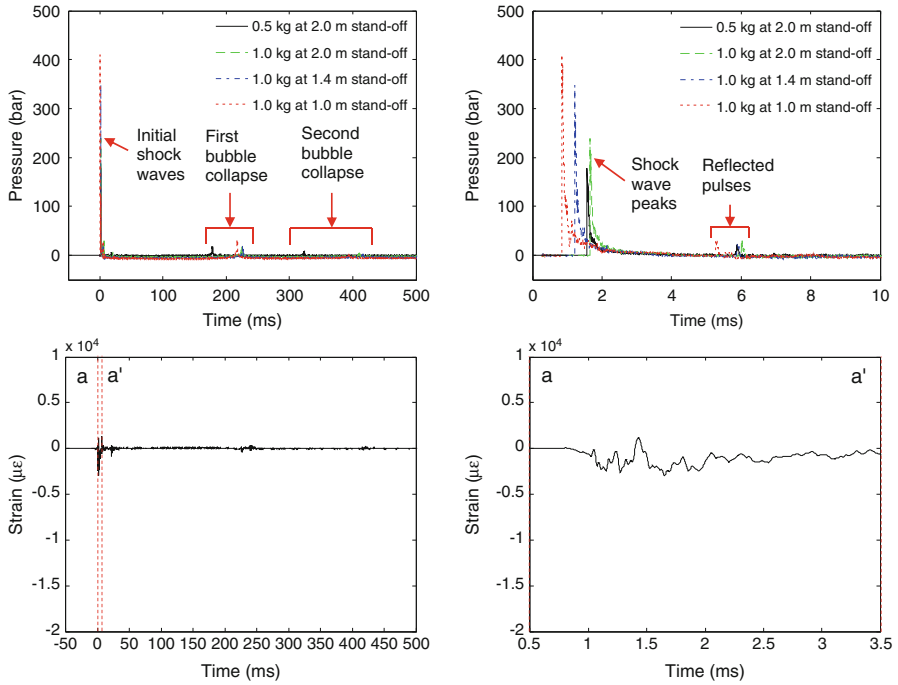


Fig. 22 Pressure–time traces for 0.5–1.0 kg blasts at stand-offs of 1.0–2.0 m: the entire event including the first bubble pulse at ~200 ms (*top left*); and initial shock pressure including reflected shock from the water surface at ~5–6 ms (*top right*). Sample strain gauge data of the tubular laminate response is given over these time periods for strain gauge position 1 monitoring axial strain (as shown in Fig. 3) of the air-filled A1 when subjected to the 1 kg charge C4 at 1.4 m stand-off

still remained intact after deflecting 80 mm. The transition to underwater studies showed different energy absorbing and failure mechanisms. Core crushing and skin fibre breakage was observed but not complete skin-to-skin failure when subjected to peak shock pressures of 450 bar. The tubes represented an alternative geometry and the variable of filler medium (water or air) proved to influence the response greatly.

5.1 Air Blast Loading of GFRP-Skinned & CFRP-Skinned Sandwich Composite Panels

A summary of the key results and observations from the air-blast loading of GFRP-skinned & CFRP-skinned sandwich panels is given in Table 2. For the Series A experiments, comparing the response of G1 (40 mm core thickness) and G2 (30 mm core thickness) it was shown that the influence of increasing the core thickness lowered the amplitude of oscillations. Increasing the core thickness increases the second moment of area of the panel and the equivalent flexural rigidity, D .

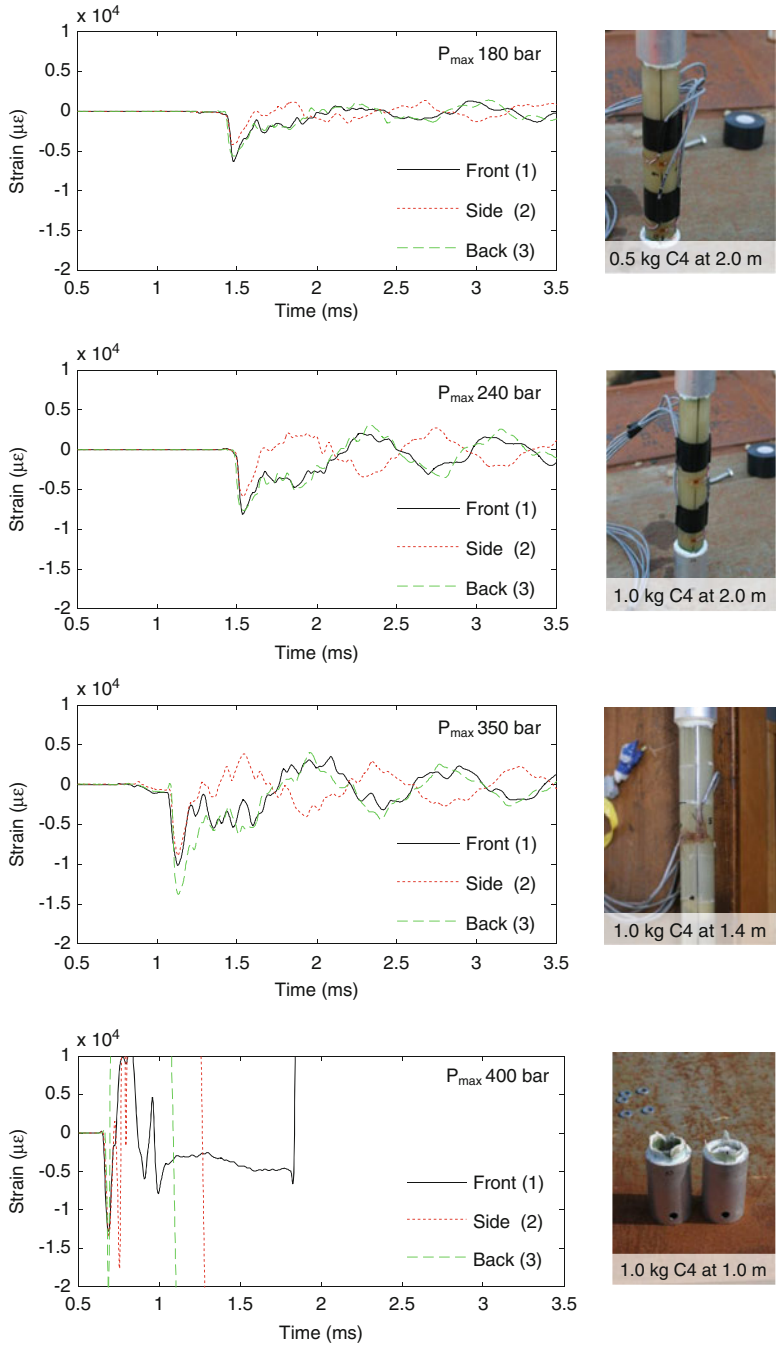


Fig. 23 Shock loading of composite tubes with max shock pressure increasing from 180 to 400 bar

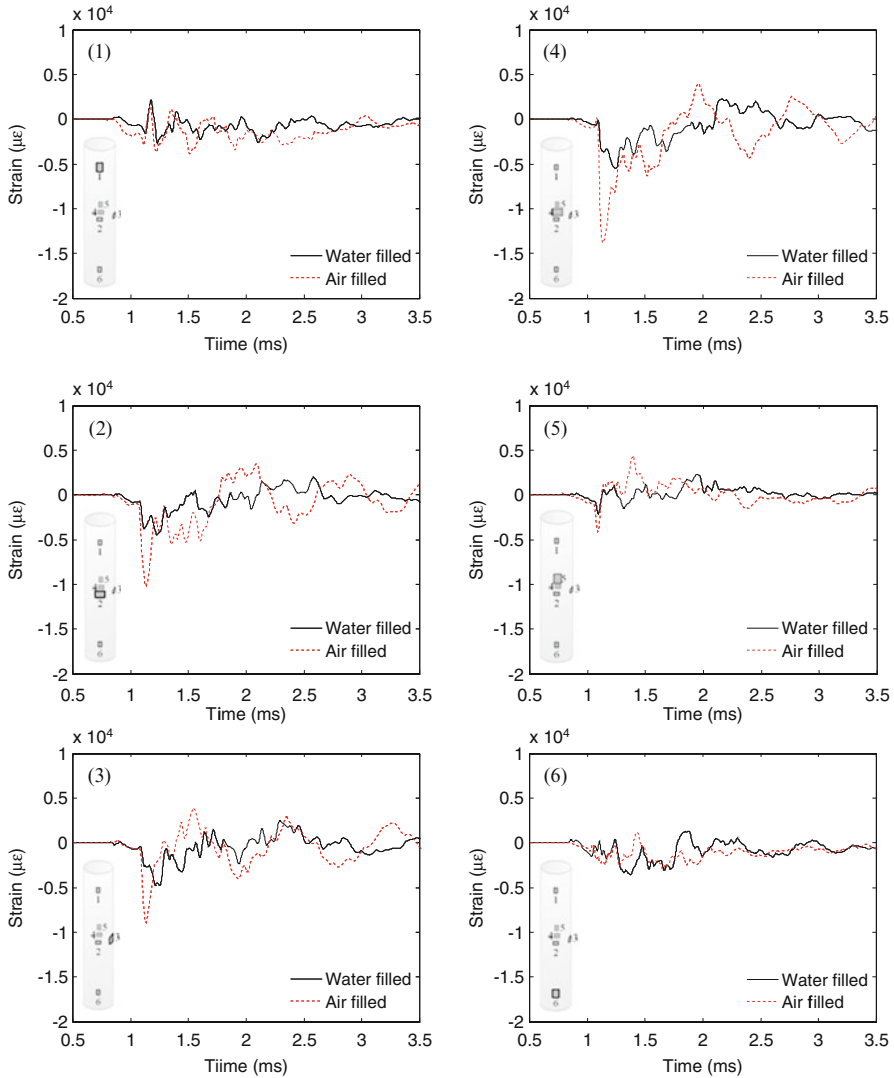


Fig. 24 Strain gauge data is displayed for the first 3.5 ms with peak shock pressure of 350 bar (1 kg C4; depth 6 m; stand-off 1.4 m) for each gauge position on tubes AF and WF, each plot shows the corresponding data for AF (air filled) and WF (water filled) at that particular location

According to [32] D is proportional to the square of the core thickness in sandwich materials. Therefore increasing the core thickness increased the stiffness of the panel and this provided for smaller peak amplitude of displacement. G1 was seen to deflect to a maximum distance out-of-plane of 63 mm whilst G2 deflected 78 mm. The first period of oscillation differed by only 10% between the two targets. Referring also to [29] discussing the response of a fully clamped panel to a uniformly distributed load,

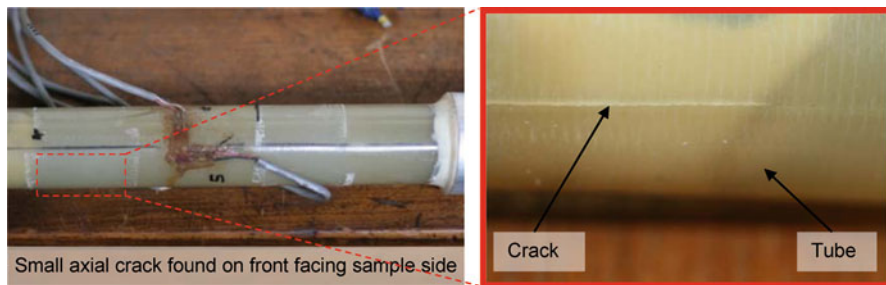


Fig. 25 Post-test images of the AF tube (peak shock pressure of 350 bar) featuring axial cracking near one end (*left*) and a zoomed in view of the crack formed during the blast (*right*)

the equivalent single degree of freedom spring constant of the panel is proportional to D . Combining this stiffness term with the mass term, the natural frequency can be determined. Therefore the period of oscillation was reduced for the thicker core, G1, given the stiffness term increased more significantly than the mass term, in this case by 10%, which was observed when referring to Figs. 6 and 7.

The second G1 panel was tested with the 30 kg charge at 8 m, it can be seen when Figs. 6 and 9 are compared that G1 deflected over twice as much as during the blast at 14 m. The increased pressure (2–8 bar peak shock pressure) and impulse (0.43–1.25 bar ms) caused a more severe response from the target. There is a deviation from static analysis where, the response of a structure to an applied load will be expected to be proportional. These load cases discussed in this paper are highly rate dependent and the structural response is nonlinear. Furthermore introducing damage (and transient boundary conditions) can affect the energy absorbing mechanisms in action and therefore the amount of energy transferred to momentum in the plate.

In terms of damage when the second G1 panel was subject to a stronger blast a skin crack formed on the front face of the target. Employing DIC was a powerful tool for damage detection during the blast. The major principal strain fields generated can tell a great deal about what is happening to the structure. Referring to Fig. 9 it is clear that there is a build up of high-strain of around 3% in the central region until a point, where there is a split in the strain field, with some strain relief appearing in a narrow region down the right-hand side of the panel. This region of stress relief indicates a region of separation between the core and skin (where the skin is unsupported by the core), resulting in the load concentrating on the edges of this (cracked-core) region on the skin. The levels of strain observed in the skin along these edges peaked at 1.8%. Further analysis in Fig. 26 displays the deformed profile of the width of the panel. Out-of-plane displacement of a horizontal central section was taken within the ARAMIS post-processing software and plotted over regular time intervals for the duration of the initial response. It shows the panel deflecting in a symmetrical manner during its inward stroke, up until the point of maximum deflection occurring at 12.5 ms. It is clear that a failure (or change in structural balance) has occurred within the panel, causing an asymmetric rebound profile of the panel at 15.5 ms.

Table 2 Summary of each air-blast conducted on GFRP- and CFRP-skinned sandwich panels highlighting the peak pressures, peak strains and visible damage

Sample code	Skin lay-up, core thickness (mm)	Charge size (kg), Stand-off distance (m)	Peak pressure (bar), duration (ms)	Peak strain (%) ^a	Damage	Notes
G1	2 × QE1200, 40 P800	30 kg; 14 m	2 bar; 6 ms	1	No visible damage	No damage detected in DIC analysis
G2	2 × QE1200, 30 P800	30 kg; 14 m	2 bar; 6 ms	1.25	No visible skin damage, some mild core cracks	Mild signs of damage visible in DIC
G1	2 × QE1200, 40 P800	30 kg; 8 m	8 bar; 5 ms	3	Severe skin and core cracking (no crushing)	Definite signs of damage shown in DIC as well as in post inspection
G3	2 × QE1200, 25 M130	100 kg; 14 m	2.5 bar; 12 ms	1.6	Severe skin and core cracking	DIC confirms appreciable defect and shows damage to front skin and core
C1	2 × RC245T & RC380T, 25 M130	100 kg; 14 m	2.5 bar; 12 ms	0.8	Slight skin crack; less severe but more widespread core cracking	DIC shows reduced deflection and minimal damage

^aStrain measurements were taken from the back face of the target

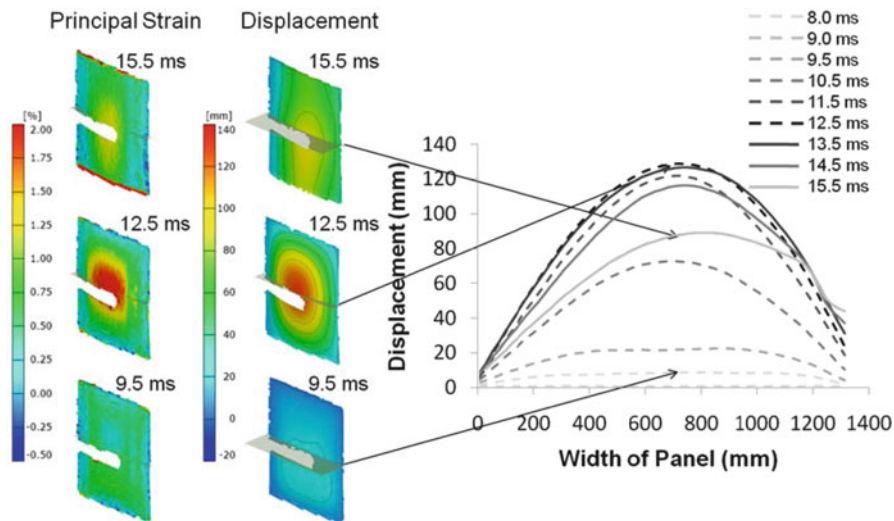


Fig. 26 Displacement data taken across a horizontal section running through the point of maximum deflection for panel G1 (core thickness 40 mm) during blast loading (30 kg at 8 m stand-off). Data displayed for several time intervals from 8 ms after detonation. *Dotted lines* show displacement profile up to maximum deflection and *solid lines* show subsequent return

This reinforces the notion of a complete core shear failure, resulting in complete crack propagation from face-to-face down a significant portion of the panel. The first 1.5 ms (8.0–9.5 ms) of response show the flat central area of the panel progressing, which is characteristic to impulsive loading situations. After 1.5 ms, there is a faint region of stress-relief on one edge of the panel due to crack initiation causing separation between the skin and core (locally). Now it can be accounted for due to the exaggerated bending stresses experienced in the early stages (around the square wave front) where the radius of curvature in the bend is significantly lower. The reason for the crack developing preferentially on one side rather than the other is due to the uneven loading experienced and the asymmetry in support conditions. The cubicle design is such that one edge of the composite sandwich panel leads to free air and one edge leads to the centre of the cubicle and so the magnitude of impulse deteriorates on one side relative to the other. This cubicle design also leads to an effectively more rigid support along the edge of the cubicle compared to the central support. For the ideal case (with the same support and loading all around the panel) cracks would be forming from all four corners causing a square section of the panel to crack. However, once one crack forms, stress relief dictates that another is unlikely to form without sustained or increased loading. Once the crack formed in the core the front (and back) skins were left unsupported by the core and therefore the strains concentrated on the edges of this core crack and this lead to skin fibre breakage. Sectioning confirmed that failures had occurred, specifically the core crack, which propagated through from face-to-face of the core (see Fig. 10). However, the DIC analysis did pick up the separation of skin and

core, also highlighted in the blast on G2 to an extent, confirmed with sectioning. With appropriate experience, DIC can be a very powerful tool for monitoring the structural integrity of various materials and identifying damage mechanisms occurring even when subject to extreme load cases such as these.

For the series B experiments, with the GFRP-skinned sandwich panels (G3), there was a uniform forward (positive) stroke, however, due to the compromised integrity of the skin and core, there was an augmented return stroke. It is also apparent that there are more uniform support conditions achieved with the use of two panels side by side. This was the aim of this test fixture, to avoid or minimise the bias on strain distributions. Although this was achieved the location of the failure occurred on one side of the target. The core crack seemed to initiate in the early stages again at ~ 1.5 ms after impact, 16.5 ms after detonation. As stated previously, the higher bending stresses cause shear cracks to initiate in the early stages of the G3 & C1's deformation cycles. However, since the GFRP-skinned panel provides less resistance to the shock wave impact, the severity of damage increases faster than in the CFRP-skinned panel. Furthermore, the average velocity of the target deformation is 40 m/s in G3 compared to 25 m/s in C1. In the case of G3 this lead to fibre breakage all along this crack at the point of peak deflection. In the CFRP target, C1, distributed the blast energy more effectively through the panel and responded with a greater resistance to the impact. It gained in less kinetic energy too, which was sustained on the rebound strike without any global skin failures. Once the centre of the target reached maximum displacement the remaining momentum carried the edges of the panel forward, unrestrained due to the loss in integrity of the core, leading to this flattening out observed of the deformed profile after the maximum displacement is reached.

Finally, S1 is analysed to give a direct comparison to the GFRP and CFRP sandwich panels. The steel plate exhibits the classic impulsive behaviour, with the central flattened region. This blast caused bolt shear to occur on one side causing the bias on the deformed profile. The plate was moving at an average velocity of 25 m/s at the point of bolt shear, causing a jump in the central point velocity (up to 31 m/s). Then this remaining tail of the pressure pulse and momentum of the plate causes the plate to continue with large plastic deformations. The steel plate is heavier than the composite sandwich panels, therefore these velocities of deformation and magnitudes of deflection are considerable from a blast mitigation point of view.

5.1.1 Accuracy of Data Reported by DIC Compared to Laser Gauge Measurements

As stated previously, point data on the targets was taken from the DIC analysis and compared to the measurements recorded by a laser gauge for verification purposes (see Fig. 27). Data was taken from the point where the laser gauge was targeting, which was precisely identified in the raw images. There was good agreement, with a $<1\%$ error until maximum deflection, between the two sets of measurements as shown in Fig. 27a.

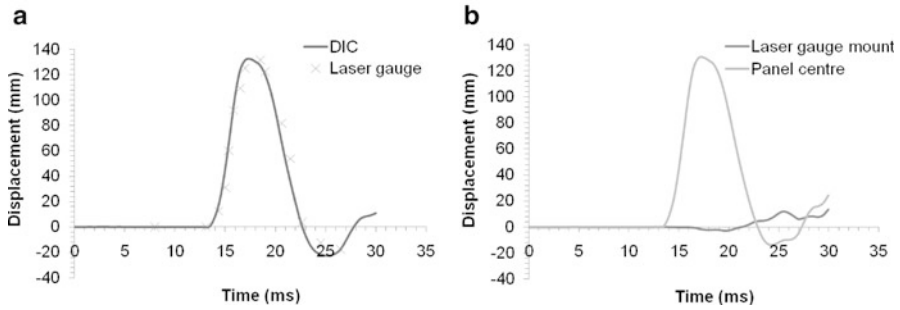


Fig. 27 Comparison of the central point displacement measured by the laser gauge and that recorded by the DIC analysis. The data shown is from the 30 kg at 8 m stand-off air-blast on G1: (a) analysis of the same point deflection during the blast measured by the DIC analysis and by the laser gauge; and (b) point data taken from the DIC analysis showing the relative movement of the laser gauge mount to its original target point on the panel

During the blast event, there reaches a point in time where the laser gauge (visibly) began to move and the data it was recording became compromised. The steel beam structure, comprising the mount for the laser gauge, flexed and vibrated after the (primary) target response reached peak deflection. To clarify when the laser gauge began to move, the steel beam itself was speckled and computed for its movements. It can be seen from Fig. 27b that the position of the laser gauge begins to move at the point where the panel is reaching its maximum deflection. This data shows qualitatively where the reliability of the data deteriorates. After this stage the laser gauge begins to flex and rotate (observed in the video recording) and so the validity of its results breaks down, since it was not at its original start position nor was it pointing at the same point. This exercise indicated a close agreement of the two systems for point displacement measurements until the point of maximum deflection. Therefore the validity of the measurements taken using DIC techniques under such extreme conditions can be taken to be true (provided vibrations of the cameras can be kept to a minimum). Provisions of heavy based tripods, held down with auxiliary weighting, supporting the cameras isolated on rubber mounts ensured minimal vibration transmission until the target's first period of oscillation completed. To be conservative within this analysis, the DIC data is accepted until the first rebound. All data presented and discussed is taken from within this period.

5.2 Underwater Blast Loading of GFRP Sandwich Composite Panels

As shown earlier with post-test images, significant damage was sustained by each target. Key observations and results are summarised in Table 3. The air-backed panel G4 (30 mm core thickness) had its core crushed to half the original thickness by the

shock with pressure 430 bar (duration is stated in Table 3 as a duration of the peak, in this case 0.2 ms, and as a duration of the tail of the shock wave, which decays at a much slower rate than the initial stage, here the tail duration is 3.2 ms). By the time typical membrane response began, excessive surface strains remained in the region of 1% causing cracks to form within the skins along the panel edges. The front surface strain measurements for gauges 4–6 are displayed in Fig. 21. From gauge 6 positioned at the top edge of the panel, it is clear that the panel bent, deformed around its edge, causing the 2–3% strains observed on the surface in that region. Comparing the strains across that length from edge to centre it is clear that after the initial compression, the centre moves into tension (unlike the panel edges), causing a possible third order mode shape of flexural response. In other words the typical impulsive shape of deformation shown previously for the air-blast trials was present, where a square profile deforms outwards upon impact prior to parabolic oscillations. The resulting visible front-face damage concentrated around the top edge is shown previously in Fig. 21. Although the initial shock can be assumed to act uniformly over the entire face, the bubble pulse would mainly have affected the top edge, given the first bubble minimum would have occurred 0.9 m above the site of the charge (calculations taken from [33]). This can account for the discrepancy of visible damage sustained by the top edge, since nearly half the explosive energy released by the charge contributes towards the pulsation of the bubble and this would have been imparted predominantly on the top edge of the panel.

For the water-backed shock loading of G5 thickness, by the shock with pressure 300 bar, it was shown that each face initially went into a state of compression, forcing the sandwich panel inwards on itself. This can be due to a number of reasons, namely, the panel being forced backwards against a mass of water and, due to the small time period and the fact that the water is encapsulated within the base-frame, this caused an initial crushing effect (on the target) as there was insufficient means for the water to vent out of the frame (seals). This caused an increased through-thickness stress on the panel compared to when the panel is backed by air, resulting in the highly compressed core. The edges of the panel peaked into tension on both faces, perhaps as a response to the compression of the core or superposition of surface stress waves at the boundary edge. After this, typical oscillatory motion ensued with strains of $\pm 0.2\%$ resulting. There was no visible damage to the skins after the blast due to the relatively low surface strains experienced. The 15 mm thick core however was crushed to nearly half its original thickness due to this pressurising effect. The difference between the two underwater blasts in terms of peak shock pressure and the backing medium meant that for the lower peak shock pressure the same relative core thickness reduction was experienced, simply due to the fact that the backing medium was denser. This phenomenon was verified in another set of trials where two targets of same thickness were subject to the same peak shock pressure with only the backing medium the variable. The air backed panel sustained more skin damage but less core crushing due to the nature of the fluid medium supporting the skins.

Table 3 Summary of each underwater blast conducted on GFRP sandwich panels highlighting the peak pressures, peak strains and visible damage

Sample code	Skin lay-up, core thickness (mm)	Stand-off distance (m)	Charge size (kg),		Peak pressure (bar), duration (ms)	Peak strain (%) ^a	Damage	Notes
			1.0, 1.4 (water-backed panel)	1.0, 1.0 (air-backed panel)				
G4	2 × QE1200, 15	1.0, 1.4 (water-backed panel)	300 bar	0.2 ms (peak)	±0.6/−0.6	Severe core crushing but no visible skin damage	Water was present behind panel ~ squashing the panel during the blast	
			0.2 ms (tail)	3.0 ms (tail)				
G5	2 × QE1200, 30	1.0, 1.0 (air-backed panel)	430 bar	0.2 ms (peak)	−3/−1 ^b	Severe core crushing and skin cracking	Air was present behind panel ~ unsupported	
			0.2 ms (tail)	3.2 ms (tail)				

^aStrain measurements are shown for the front and back face of the target^bStrain gauges lost the recording after the initial impact caused a given state of strain (compression)

5.3 *Underwater Blast Loading of GFRP Tubular Laminates*

The results are summarised in Table 4 for both the progressive loading of GFRP tubular laminates as well as the experiments to observe the effect of the filler medium.

5.3.1 **Progressive Shock Loading of GFRP Tubular Laminates**

This set of blasts produced progressive damage on the tube constructions from no visible damage to complete shear failure, when subjected to peak shock pressures of 180–400 bar. For the blast of 0.5 kg at 2 m producing a peak shock pressure of 180 bar, 0.1 ms duration, the gauge data indicated mild bending response with opposing axial strain gauges recorded signals that were out-of-phase with each other i.e. one in tension when the other is in compression; and initial breathing action hoop strains were all in compression (-0.6%). After this (0.5 ms after impact) the tube response reverts to an oscillatory squashing motion (front/back strain gauges were out-of-phase with side strain gauges), see Fig. 16 for hoop strain data.

This air filled (AF) construction was tested to a peak shock pressure of 240 bar, 0.1 ms duration, (1.0 kg at 2 m stand-off). This blast resulted in larger amplitude of strains of similar characteristics to the previous blast (0.5 kg at 2 m). Strains peaked at 0.8% across the range of gauges. There were generally only mild signs of possible damage with chalky patches appearing on the tube surfaces (mild matrix cracking). This was the threshold for damage for this construction. The AF tube was then subject to a peak pressure loading of 350 bar, 0.1 ms duration, (1.0 kg at 1.4 m stand-off), which resulted in axial cracks forming at the front ends of the tubes. The characteristic response of the tube was again similar to that those tested previously with strain peaking at 1.5%, highlighted in Fig. 16. The final blast, 1 kg at 1 m stand-off, on AF tubes exceeded the blast limit of the tube construction when subject to a peak pressure of 400 bar, 0.2 ms duration. From the strain data in Fig. 16 it is clear that the tubes response was insufficient to absorb the energy imparted on it in a quick enough period. The strain gauge recordings implied an initial compression inwards, with the front face circumferential gauge holding at 0.5% strain, prior to the ends of the tube shearing away from the fixed end-tabs, terminating all recordings within the first 5 ms.

5.3.2 **Effect of Filler Fluid on Tubular Laminate Response**

All common modes of response expected by tube structures to underwater shocks were present as mentioned in the previous section of analysis: circumferential reduction/expansions (breathing) and elliptical oscillations (squashing) as illustrated in Fig. 28. The tubes represent an alternative geometry to the flat panels. The initial shock wave wraps around the cylindrical geometry, causing an inward compression. After the pressure of the surrounding fluid reduces the energy gone into deforming

Table 4 Summary of each underwater blast on GFRP tubular laminates highlighting the peak pressures, peak strains and visible damage

Sample code	Charge size (kg),		Peak pressure (bar), duration (ms)	Peak strain (%) ^a	Damage	Notes
	Stand-off distance (m)					
AF	0.5, 2.0		180 bar 0.1 ms (peak) 2.4 ms (tail)	-0.2/0.3/±0.2	No visible damage	Elastic oscillations
AF	0.5, 2.0		180 bar 0.1 ms (peak) 2.4 ms (tail)	-0.6/-0.6/-0.4	No visible damage	Elastic oscillations
AF	1.0, 2.0		240 bar 0.1 ms (peak) 2.3 ms (tail)	-0.4/0.4/±0.3	Some surface fibre damage visible	Elastic oscillations but subsurface damage to laminate
AF	1.0, 2.0		240 bar 0.1 ms (peak) 2.3 ms (tail)	-0.7/-0.8/-0.5	Some surface fibre damage visible	Breathing motion clearly observed with larger amplitude strains
AF	1.0, 1.0		400 bar 0.2 ms (peak) 3.0 ms (tail)	±1/+ve/+ve ^b	Complete shear failure at the ends of the tube	The central section began to respond prior to fracture at ends
AF	1.0, 1.0		400 bar 0.2 ms (peak) 3.0 ms (tail)	±1/3/±1 ^b	Complete shear failure at the ends of the tube	The central section began to respond prior to fracture at ends
AF	1.0, 1.4		350 bar 0.1 ms (peak) 2.3 ms (tail)	-1/-1.5 -1	Axial cracking at front face ends of tubes	Hoop strains dominated with larger amplitude of strains
WF	1.0, 1.4		350 bar 0.1 ms (peak) 2.3 ms (tail)	±0.3/-0.5 -0.4	No visible damage	Filler fluid damped the strains experienced

^aStrain measurements are shown for the front, back and side of each tube^bStrain gauges lost the recording after the initial impact caused a given state of strain (tension)

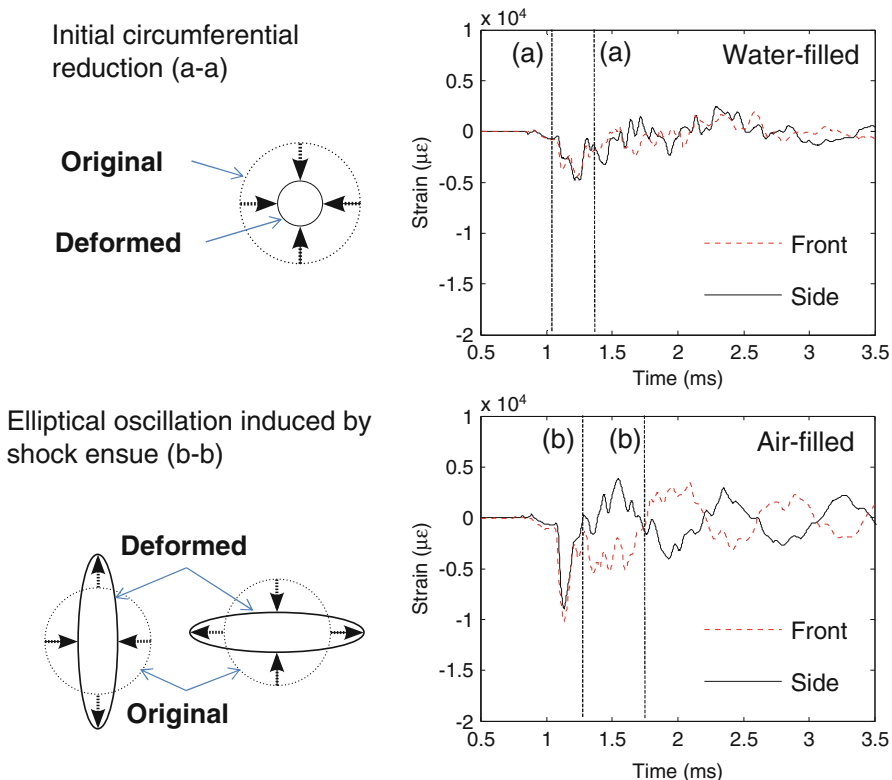


Fig. 28 Diagram illustrating the two main modes of deformation observed, breathing (*top left*) and elliptical oscillation or squashing (*bottom left*) as the relative magnitudes of strain observed in both tube cases, water filled (*top right*) and air-filled (*bottom right*)

the tube in this manner is released in the mode of oscillatory vibrations with the dominant mode in the form of a circumferential squashing motion. These two modes of vibration were the most dominant of those observed during these trials, however, the most significant result to emerge from this trial is the fact that the backing fluid (filler fluid) made considerable savings with regard to damage sustained by the tube structures (visible in Fig. 25). The denser filler medium (water) made the tube effectively more rigid and reduced the magnitude of surface strains experienced and hence damage sustained. Figure 24 shows that the water filled tube experienced surface strains of half the magnitude of those experienced by the air-filled tube. To analyse this further, having a denser filler medium also dampens the vibrations quicker. After a few milliseconds, the strains in the air-filled tube are still greater than even the maximum strain experienced by the water filled tube. Moreover the water-filled tube seems to also resist the elliptical/squashing mode of vibration clearly observed with the air-filled tube. This is due to the fact that the tube needs to compress the filler medium to oscillate between tension/compression when going

through this squashing motion and the energy required to compress the denser filler medium is too great. Therefore the energy is dissipated within the water filler medium and in mild residual surface vibrations in comparison to the air-filled tube which freely vibrates with large magnitude of strains $>1\%$ (highlighted in Fig. 28).

6 Conclusions

These sets of blast data have shown the capabilities of simple composite constructions to resist blast loads. Both conventional (strain gauges) and more advanced (high-speed DIC) strain monitoring techniques were employed to monitor the deformation of the targets during the blasts. Various aspects of blast events have been highlighted by these studies such as the ferocity of these explosions, the damage they can inflict as well as how boundary conditions can affect the outcome in terms of damage sustained and how these boundary conditions can play more of an important role in blast mitigation than material design.

These experiments were conducted on commercially available marine constructions, on a large scale (target length scales in the range of 0.3–1.6 m) against actual explosive charges (0.64–100 kg TNT equivalent charge weights). These experiments differ from others investigating blast/shock impact on such materials, due to the style of tests approaching a real simulation of in-service conditions (large-scale targets subject to explosions both in-air and underwater).

During the underwater blast experiments the sandwich panels were subject to pressures over 100 times greater in magnitude in less than a tenth of the period of time than those experienced during the air-blast experiments. During the air-blast experiments, back-face skins (and front-face skins generally) maintained their form without tearing/cracking. However during the underwater blasts, the cores experienced considerable crushing (up to 50%) and the skins experienced very large strains, causing fibre breakage on both faces (with strains exceeding 3%) when the targets were backed by air. The effect of having water as a backing medium reduced the surface strains experienced and hence damage incurred by the skins but increased the relative crushing observed in the core. Tube structures were tested and the effect of the filler/backing medium was again apparent with the water filled tube reducing surface stains by 60% in some regions. The sample data is limited for traditional statistical analysis of sample response (no repeat experimentation). This is due to the fact that the samples used were full-scale (up to 1.3 m \times 1.6 m for air blasts) and restrictions were in place with respect to the consumables required to manufacture them. However, within the small sample of tests conducted, verification of the data collected for the air-blasts was achieved to some extent using two techniques for point measurement and for the underwater-blasts using multiple gauge arrangements, giving confidence in the quality of data recorded.

The main findings in summary are:

- DIC was successfully employed during full-scale air-blast experiments to capture the damage progression in sandwich structures.

- CFRP-skinned sandwich panels exhibited less damage and deformation than equivalent GFRP-skinned sandwich panels when subject to explosive air blast.
- There is a difference in response of GFRP sandwich panels to air-blast (30 kg at 8–14 m) and underwater-blast loading (1.0 kg at 1.0–1.4 m) due to the different pressure–time signatures: peak shock pressures of 2–8 bar (6 ms duration) to 300–430 bar (0.2 ms duration).
- Damage mechanisms changed from front-face skin damage and core shear cracking for air blast to severe core crushing (up to 50%) and skin fibre-breakage for underwater blast.
- Damage and response of tubes subjected to underwater blast varies according to whether the tubes are filled with air or water, with the air-filled tubes sustaining longitudinal cracking compared to no visible damage on the water-filled tube subject to the same blast load.
- All experiments, on blast loading of GFRP and CFRP-skinned composite structures, highlighted the importance of boundary conditions on the structural response and damage sustained by the structure, in terms of both location and nature of damage caused by a blast.

Acknowledgements Much appreciated is the strong support received from Dr Yapa Rajapakse of the Office of Naval Research (ONR N00014-08-1-1151) in particular for Hari Arora. We also acknowledge the Metropolitan Police and CPNI for use of the test cubicles and other equipment, GL Industrial for the use of their facilities and support on site, SP Gurit for provision of materials and GOM mbH for access to latest DIC equipment during the air-blast trials and Shouhua Chen and Paolo Del Linz for help with analysis of DIC and other experimental results.

References

1. Ambrosini RD, Jacinto AC, Danesi RF (2001) Experimental and computational analysis of plates under air blast loading. *Int J Impact Eng* 25(10):927–947
2. Hoo Fatt MS, Palla L (2009) Analytical modeling of composite sandwich panels under blast loads. *J Sandw Struct Mater* 11(4):357–380
3. Neuberger A, Peles S, Rittel D (2007) Scaling the response of circular plates subjected to large and close-range spherical explosions. Part I: air-blast loading. *Int J Impact Eng* 34(5):859–873
4. Neuberger A, Peles S, Rittel D (2007) Scaling the response of circular plates subjected to large and close-range spherical explosions. Part II: buried charges. *Int J Impact Eng* 34(5):874–882
5. Menkes SB, Opat HJ (1973) Tearing and shear failure in explosively loaded clamped beams. *Exp Mech* 13(11):480–486
6. Nurick GN, Martin JB (1989) Deformation of thin plates subject to impulsive loading – a review. Part II: experimental studies. *Int J Impact Eng* 8(2):171–186
7. Nurick GN, Olsson MD, Fagnan JR (1993) Deformation and rupture of blast loaded square plates – predictions and experiments. *Int J Impact Eng* 13(2):279–291
8. Gelman ME, Nurick GN, Marshall NS (1986) Tearing of blast loaded plates with clamped boundary conditions. *Int J Impact Eng* 18(7–8):803–827
9. Nurick GN, Simmons MC, Cantwell WJ, Langdon GS, Lemanski SL, Schleyer GK (2007) Behaviour of fibre-metal laminates subjected to localised blast loading: Part I experimental observations. *Int J Impact Eng* 34:1202–1222

10. Langdon GS, Simmons MC, Cantwell WJ, Lemanski SL, Nurick GN, Schleyer GK (2007) Behaviour of fibre-metal laminates subjected to localised blast loading: Part II experimental observations. *Int J Impact Eng* 34:1223–1245
11. Cantwell WJ, Langdon GS, Nurick GN (2005) The blast response of novel thermoplastic-based fibre-metal laminates some preliminary results and observations. *Compos Sci Technol* 65: 861–872
12. Tekalur SA, Shivakumar K, Shukla A (2008) Mechanical behavior and damage evolution in E-glass vinyl ester and carbon composites subjected to static and blast loads. *Compos Part B Eng* 39(1):57–65
13. Tekalur SA, Bogdanovich AE, Shukla A (2009) Shock loading response of sandwich panels with 3-D woven E-glass composite skins and stitched foam core. *Compos Sci Technol* 69(6):736–753
14. Tekalur SA, Shukla A, Shivakumar K (2008) Blast resistance of polyurea based layered composite materials. *Compos Struct* 84(3):271–281
15. Wang EH, Shukla A (2010) Analytical and experimental evaluation of energies during shock wave loading. *Int J Impact Eng* 37(12):1188–1196
16. Jackson M, Shukla A (2011) Performance of sandwich composites subjected to sequential impact and air blast loading. *Compos Part B Eng* 42(2):155–166
17. Cole RH (1948) *Underwater explosions*. Princeton Univ. Press, Princeton
18. Hetherington JG, Smith PD (1994) *Blast and ballistic loading of structures*. Butterworth Heinmann, Oxford/Boston
19. Panciroli R, Abrate S (2009) Dynamic response of sandwich shells to underwater blasts. In: ICCM 17, IOM Communications, Edinburgh
20. Deshpande VS, Heaver A, Fleck NA (2006) An underwater shock simulator. *P R SocA Math Phys Eng Sci* 462(2067):1021–1041
21. Espinosa HD et al (2009) Performance of composite panels subjected to underwater impulsive loading. In: ONR 2009 solid mechanics program, UMUC, Maryland
22. LeBlanc J, Shukla A (2010) Dynamic response and damage evolution in composite materials subjected to underwater explosive loading: an experimental and computational study. *Compos Struct* 93(3):1060–1071
23. Ravichandran G, Bhattacharya K, Colonius T, Dimotakis PE, Gharib M, Ortiz M, Rosakis AJ, Shephard JE (2009) Muri on mechanics and mechanisms of impulse loading, damage and failure of marine structures and materials. In: Rajapakse JY (ed) ONR solid mechanics program 2009. UMUC, MD
24. Arora H, Hooper PA, Dear JP (2011) Dynamic response of full-scale sandwich composite structures subject to air-blast loading. *Compos Part A* 42:1651–1662
25. Bland PW, Dear JP (2001) Observations on the impact behaviour of carbon-fibre reinforced polymers for the qualitative validation of models. *Compos Part A* 32(9):1217–1227
26. Dear JP, Lee H, Brown SA (2005) Impact damage processes in composite sheet and sandwich honeycomb materials. *Int J Impact Eng* 32(1–4):130–154
27. Dear JP, Brown SA (2003) Impact damage processes in reinforced polymeric materials. *Compos Part A* 34(5):411–420
28. Rajendran R, Paik JK, Lee JM (2007) Of underwater explosion experiments on plane plates. *Exp Tech* 31(1):18–24
29. Biggs JM (1964) *Introduction to structural dynamics*. McGraw-Hill Book Company, New York
30. Deegan M (2010) Personal communication, Vishay Measurements Group, UK
31. Kwon YW, Fox PK (1993) Underwater shock response of a cylinder subjected to a side-on explosion. *Comput Struct* 48(4):637–646
32. Gibson LJ, Ashby MF (1997) *Cellular solids, structure and properties*, 2nd edn, Cambridge solid state science. Cambridge University Press, Cambridge
33. Reid WD (1996) *The response of surface ships to underwater explosions*. Department of Defence, Defence Science and Technology Organisation, Melbourne